Article

Developmental Cell

Combining Developmental and Perturbation-Seq Uncovers Transcriptional Modules Orchestrating Neuronal Remodeling

Graphical Abstract

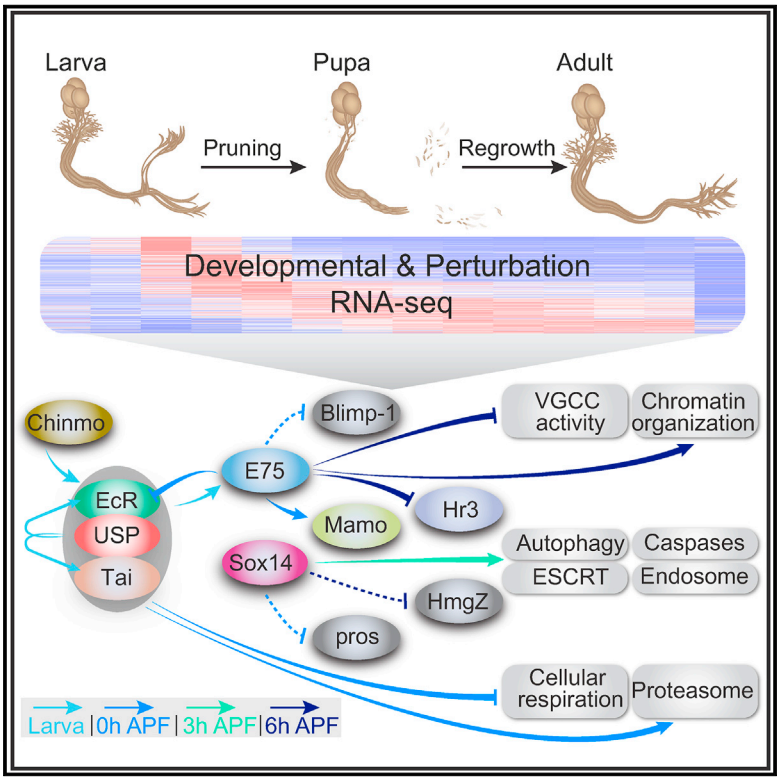

Highlights

- A developmental expression atlas of MB γ neurons highlights remarkable dynamics
- We uncovered 7 DNA binding proteins (DBPs) that regulate neuronal remodeling
- Sequencing perturbed neurons identified a hierarchical transcription factor network
- Superimposing developmental and perturbation-seq identifies key downstream modules

Authors

Idan Alyagor, Victoria Berkun, Hadas Keren-Shaul, ..., Noa Issman-Zecharya, Ido Amit, Oren Schuldiner

Correspondence

oren.schuldiner@weizmann.ac.il

In Brief

Developmental processes are often transcriptionally regulated. Alyagor et al. dissected the transcriptional landscape of a distinct neuronal type undergoing stereotypical remodeling in fine-grained temporal resolution. Superimposing this developmental expression atlas on profiles of neurons mutant for key transcription factors revealed a hierarchical regulatory network.

Alyagor et al., 2018, Developmental Cell *47*, 38–52
October 8, 2018
https://doi.org/10.1016/j.devcel.2018.09.013

CellPress

CellPress

Developmental Cell
Article

Combining Developmental and Perturbation-Seq Uncovers Transcriptional Modules Orchestrating Neuronal Remodeling

Idan Alyagor,[1] Victoria Berkun,[1] Hadas Keren-Shaul,[2,3] Neta Marmor-Kollet,[1] Eyal David,[2] Oded Mayseless,[1] Noa Issman-Zecharya,[1] Ido Amit,[2] and Oren Schuldiner[1,4,*]

[1]Department of Molecular Cell Biology, Weizmann Institute of Sciences, Rehovot, Israel
[2]Department of Immunology, Weizmann Institute of Sciences, Rehovot, Israel
[3]Life Science Core Facility, Weizmann Institute of Sciences, Rehovot, Israel
[4]Lead Contact
*Correspondence: oren.schuldiner@weizmann.ac.il
https://doi.org/10.1016/j.devcel.2018.09.013

SUMMARY

Developmental neuronal remodeling is an evolutionarily conserved mechanism required for precise wiring of nervous systems. Despite its fundamental role in neurodevelopment and proposed contribution to various neuropsychiatric disorders, the underlying mechanisms are largely unknown. Here, we uncover the fine temporal transcriptional landscape of *Drosophila* mushroom body γ neurons undergoing stereotypical remodeling. Our data reveal rapid and dramatic changes in the transcriptional landscape during development. Focusing on DNA binding proteins, we identify eleven that are required for remodeling. Furthermore, we sequence developing γ neurons perturbed for three key transcription factors required for pruning. We describe a hierarchical network featuring positive and negative feedback loops. Superimposing the perturbation-seq on the developmental expression atlas highlights a framework of transcriptional modules that together drive remodeling. Overall, this study provides a broad and detailed molecular insight into the complex regulatory dynamics of developmental remodeling and thus offers a pipeline to dissect developmental processes via RNA profiling.

INTRODUCTION

Neuronal remodeling is a fundamental process required for the proper wiring of adult nervous system connectivity, both in vertebrates and invertebrates (Yaniv and Schuldiner, 2016; Schuldiner and Yaron, 2015; Luo and O'Leary, 2005). Remodeling often includes a degenerative phase, such as neurite or synapse elimination, as well as a regenerative phase, such as the regrowth of axons and dendrites to form new connections (Schuldiner and Yaron, 2015; Luo and O'Leary, 2005). Defects in remodeling have been hypothesized to underlie various neuropsychiatric diseases, including schizophrenia and autism (Cocchi et al., 2016; Thomas et al., 2016) and, indeed, some molecular similarities have recently been identified (Sekar et al., 2016). Therefore, a comprehensive understanding of the mechanisms that regulate developmental neuronal remodeling might shed light on the etiology of some neurodegenerative and neuropsychiatric disorders.

Many *Drosophila melanogaster* neurons undergo stereotypic remodeling during metamorphosis (Truman, 1990), thus providing a unique and genetically amenable model to dissect the cellular and molecular mechanisms underlying this process. The mushroom body (MB) comprises three sequentially born neuronal sub-populations (γ, α′/β′, and α/β), out of which only the first-born γ neurons undergo remodeling in a spatially and temporally stereotypic manner (Lee and Luo, 1999). After their initial larval growth, MB dendrites and axons undergo pruning during early metamorphosis and subsequently regrow new projections, which form the medial, adult-specific γ lobe (Figure 1A). While significant progress in our understanding of the molecular pathways underlying remodeling has been achieved (Yaniv and Schuldiner, 2016; Yu and Schuldiner, 2014), more pathways await discovery, and many aspects of the known pathways, including their regulators and downstream executers, are still unknown.

The nuclear receptor (NR) ecdysone receptor B1 (EcR-B1) has been demonstrated to be cell-autonomously required for the initiation of MB γ neuron pruning, together with its co-receptor Ultraspiricle (usp; Figure 1A; Lee et al., 2000). EcR-B1 has also been shown to be required for dendrite pruning of the sensory dendritic arborization (da) neurons (Kuo et al., 2005; Williams and Truman, 2005), as well as for the remodeling of the olfactory projection neurons (PNs) (Marin et al., 2005) and thoracic ventral (TV) neurons (Schubiger et al., 1998), suggesting that in the fly, it is a master regulator of developmental remodeling across neural systems. We have previously shown that another NR complex, comprising Unfulfilled (UNF; also known as Hr51 or Nr2e3) and Eip75B (also known as E75), regulates developmental axon regrowth of MB γ neurons following pruning (Figure 1A; Rabinovich et al., 2016; Yaniv et al., 2012). Because NRs function as ligand-dependent transcription factors (TFs), these observations together suggest that remodeling of MB neurons is mediated, at least in part, by a developmentally regulated transcriptional program.

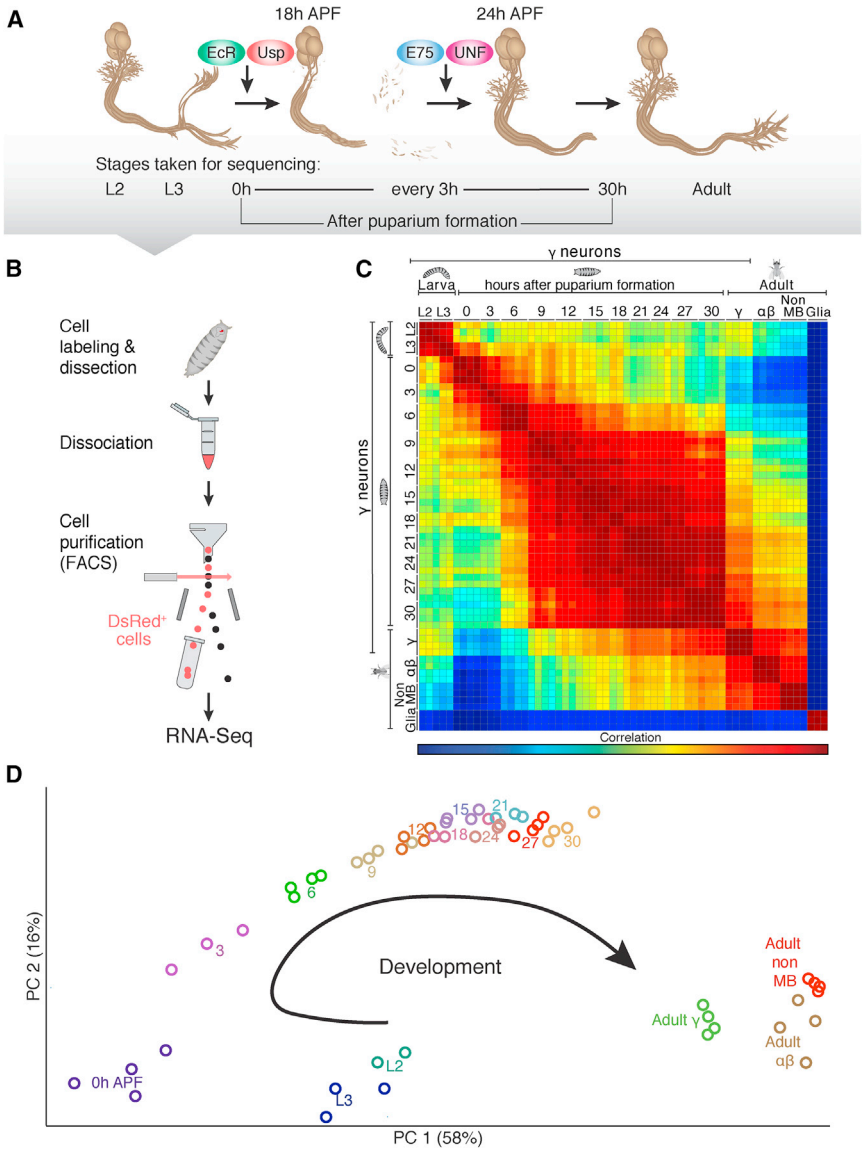

Figure 1. Expression Profiles of Developing Neurons Reveal a Dynamic Transcriptional Landscape

(A) Schematic representation of MB γ neuron remodeling and its regulation by the nuclear receptor (NR) complexes. The time-points taken for RNA-seq are indicated below. L2 and L3 refer to 2nd and 3rd instar larva, respectively.

(B) Schematic representation of the strategy we employed to isolate γ neurons from fly brains at different developmental stages.

(C) Global correlation matrix of the expression profiles indicated. We sequenced MB γ neurons at 14 developmental stages, as well as adult α/β MB neurons (labeled using NP3061-Gal4), non-MB neurons (labeled by c155-Gal4 combined with MB247-Gal80), and astrocyte-like cells (labeled by alrm-Gal4; marked as Glia).

(D) Principal-component analysis (PCA) of the neural expression profiles shown in (C). Numbers indicate hours after puparium formation (APF).

Here, we map the developmental expression atlas of MB γ neurons, specifically focusing on the developmental stages that are relevant for neuronal remodeling. We sequenced highly purified populations of isolated MB γ neurons and performed RNA sequencing (RNA-seq) to uncover the expression profiles of neurons undergoing remodeling at unprecedented temporal resolution. Using this developmental expression atlas, combined with genetic analyses, we identified specific DNA binding proteins (DBPs) as regulators of diverse aspects of neuronal remodeling. Furthermore, we have conducted a developmental perturbation-seq by sequencing γ neurons perturbed in three key TFs. Superimposing these sequencing results with the fine developmental expression atlas, we have uncovered a complex hierarchy of DBPs that contains both positive and negative feedback loops that are likely important to time and fine-tune remodeling. Moreover, it allowed us to uncover the key developmental processes and cellular pathways that together culminate in γ neuron remodeling. More generally, our easily accessible temporal-developmental expression atlas can now serve the community in delving deeper into the unknown aspects of MB development, as well as form a platform for comparison with other remodeling paradigms.

RESULTS

Expression Profiles of Developing MB γ Neurons Reveal a Dynamic Transcriptional Landscape

Remodeling of MB γ neurons requires distinct NR complexes at different steps that function as ligand-dependent TFs (Figure 1A), suggesting that a transcriptional network underlies this complex developmental process. In order to uncover the transcriptional dynamics of developing MB γ neurons, we established a multi-step process to isolate distinct populations of cells from intact brains during development, which were then used to generate high-quality sequencing libraries (Figure 1B). We expressed nuclear DsRed (RedStinger) driven by the GMR71G10-Gal4 driver (hereafter referred to as 71G10), which we found to be specifically expressed in MB γ neurons throughout development (Figure S1) but not in non-MB cells within the central nervous system. To this end, we dissected brains, dissociated them into single cells, and isolated DsRed-positive cells using a fluorescence-activated cell sorter (FACS) (Figures 1B and S2A–S2D). As controls, we isolated adult α/β MB neurons (labeled by the NP3061-Gal4), as well as adult non-MB neurons (labeled by pan neuronal C155-Gal4 additionally expressing the MB-specific repressor, MB247-Gal80, to exclude MB expression) and adult astrocyte-like cells (labeled by Alrm-Gal4). We combined our method with a sensitive and high throughput RNA-seq technology originally developed for single-cell RNA-seq applications (Jaitin et al., 2014; see STAR Methods). MB γ neurons are considered

relatively homogenous and because we aimed to extract a deep developmental expression profile at each time point, we decided to sequence pools of cells rather than single isolated neurons. In order to evaluate how many cells are needed and whether using pools of cells indeed results in robust and reproducible data, we conducted RT-PCR experiments (data not shown) with 500–1,000 neurons. Indeed, we obtained robust and reliable data from these experiments, and since 1,000 neurons are easily obtainable from 3–4 dissected brains, we decided to use pools of 1,000 cells as a starting point for all of our RNA-seq experiments. The high correlation between experimental repeats confirmed that this strategy resulted in robust data (Pearson's correlation, r = 0.94–0.99; Figure 1C). Using these methods, we sequenced RNA from MB γ neurons isolated at 14 developmental time points spanning the key transitions during developmental remodeling (Figure 1A), essentially forming a temporal-developmental expression atlas.

Correlation analysis of the transcriptional state of MB γ neurons across development and compared to other cells (Figure 1C) demonstrates that MB γ neurons undergo a developmentally regulated transcriptional program and highlights several important observations:

(1) As expected, the expression pattern of astrocytes (glia) was dramatically different from neuronal expression patterns. (2) We noticed dramatic changes in the global expression patterns, even when comparing samples only 3 hr apart, mainly during larval to pupal transition. The global correlation between adjacent time points is r = 0.80–0.94 between L3 and 9 hr after puparium formation (APF), while it is r = 0.98–0.99 between 9 hr and 30 hr APF. (3) To our surprise, the transcriptome of adult γ neurons was globally more similar to the transcriptome of other adult (even non-MB) neurons than to that of younger γ neurons. In order to better visualize these transitions, we performed a principal-component analysis (PCA) that clearly demonstrates the higher similarity of adult MB neurons to other adult neurons (Figure 1D). This result emphasizes that the developmental age of a cell plays a more dominant role than its identity in the global RNA expression pattern and also implies that the expression of so-called "cell identity markers" may dramatically change along development. Additionally, the PCA nicely demonstrates the dramatic changes in global expression between larval and early pupal stages (L2 to 9 hr APF) followed by more gradual, though unidirectional, changes in global expression trends between 9 to 30 hr APF.

In conclusion, we devised a protocol to isolate distinct populations of neurons from an intact brain during development and extract their expression profiles using RNA-seq. Our detailed temporal analyses of MB neurons revealed a dramatic transcriptional transition during metamorphosis.

Developmental Expression Atlas Highlights Axon Remodeling Gene Network

Our dataset includes reads from 11,443 distinct genes across cell types and 11,046 in γ neurons, out of which, 5,211 genes exhibited 50 reads or more in at least two γ neuron samples and were therefore considered as "significantly expressed" in γ neurons (Figure 2A). In order to classify developmentally regulated patterns of gene expression, we focused on genes whose expression was statistically dynamic during development ($p < 0.01$) and in addition demonstrated at least 2-fold differences in expression (STAR Methods and Table S1). Using these criteria, 2,671 of the genes, which account for more than half of the significantly expressed genes, exhibited dynamic expression during development (Figure 2A). Given that the developmental window we used in our experiments starts after embryonic development and major events that control differentiation and wiring of the larval γ neurons, this large proportion of genes undergoing dynamic expression was surprising.

Among the dynamically expressed genes, we identified many with known neurodevelopmental function. For example, the expression of the key regulator of remodeling in many *Drosophila* neurons, *EcR* (Kuo et al., 2005; Marin et al., 2005; Williams and Truman, 2005; Lee et al., 2000), peaks at the late larval stage (Figure 2B), consistent with its peak protein expression at the onset of pupation (Truman et al., 1994). Likewise, *headcase* (*hdc*) and *Sox box protein 14* (*Sox14*; Figure 2B), two EcR targets that were found to be required for the dendrite pruning of the da sensory neurons (Loncle and Williams, 2012; Kirilly et al., 2009), both exhibit expression peaks at the onset of the pupal stage, consistently lagging behind the peak expression of *EcR*. Similarly, the expression of *Mical* (Figure 2B), a Sox14-regulated gene required for dendrite pruning (Kirilly et al., 2009), also peaks at 0 hr APF. Interestingly, both *hdc* and *Mical* were shown not to be required for MB γ axon pruning (Loncle and Williams, 2012; Kirilly et al., 2009). The expression patterns that we reveal here suggest that in MB neurons *hdc* and *Mical* are likely targets of EcR and Sox14, respectively, but functional redundancy with unknown genes might obscure their function during MB remodeling. On the other hand, the expression of the regrowth-related gene *UNF* increases gradually, peaking at 9 hr APF while maintaining high levels during late pupa (Figure 2B). Taken together, these expression profiles validate known expression patterns of key remodeling genes and demonstrate the capability of our dataset to highlight remodeling-related genes due to their dynamic expression pattern.

In order to classify groups of genes with similar expression patterns, we performed k-means clustering (k = 10; STAR Methods), which resulted in groups of genes with distinct developmental expression profile dynamics (Figure 2C). For example, genes in clusters I and II are highly expressed in larva but their expression decreases at the onset of pupation. In each of these clusters, we identified distinct biological processes, as reflected by enrichment analyses of GO, KEGG, and Reactome terms (Figure 2C; Tables S2 and S3). For example, most of the proteasome subunits (94%) exhibit a highly similar expression pattern and clustered together in cluster III, exhibiting a peak expression at the onset of puparium (Figures 2C and 2D; Table S2). This expression is consistent with previous reports (Hoopfer et al., 2008), where the expression of proteasome subunits occurs a few hours before the onset of pruning and fits the known role of the proteasome subunits *Mov34 (Rpn8)* and *Rpn6* in MB axon pruning (Watts et al., 2003). In cluster IV, which exhibits peak expression at 3 hr APF, we found a significant enrichment in endosomal genes, and more specifically a module of genes from the endosomal sorting complexes required for transport (ESCRT) (Figures 2C, 2D, and S3A; Table S2), which were shown to be required for axon pruning of MB neurons (Issman-Zecharya and Schuldiner, 2014) as well as da dendrites (Loncle et al., 2015; Zhang et al., 2014). In the same cluster, we found enrichment of

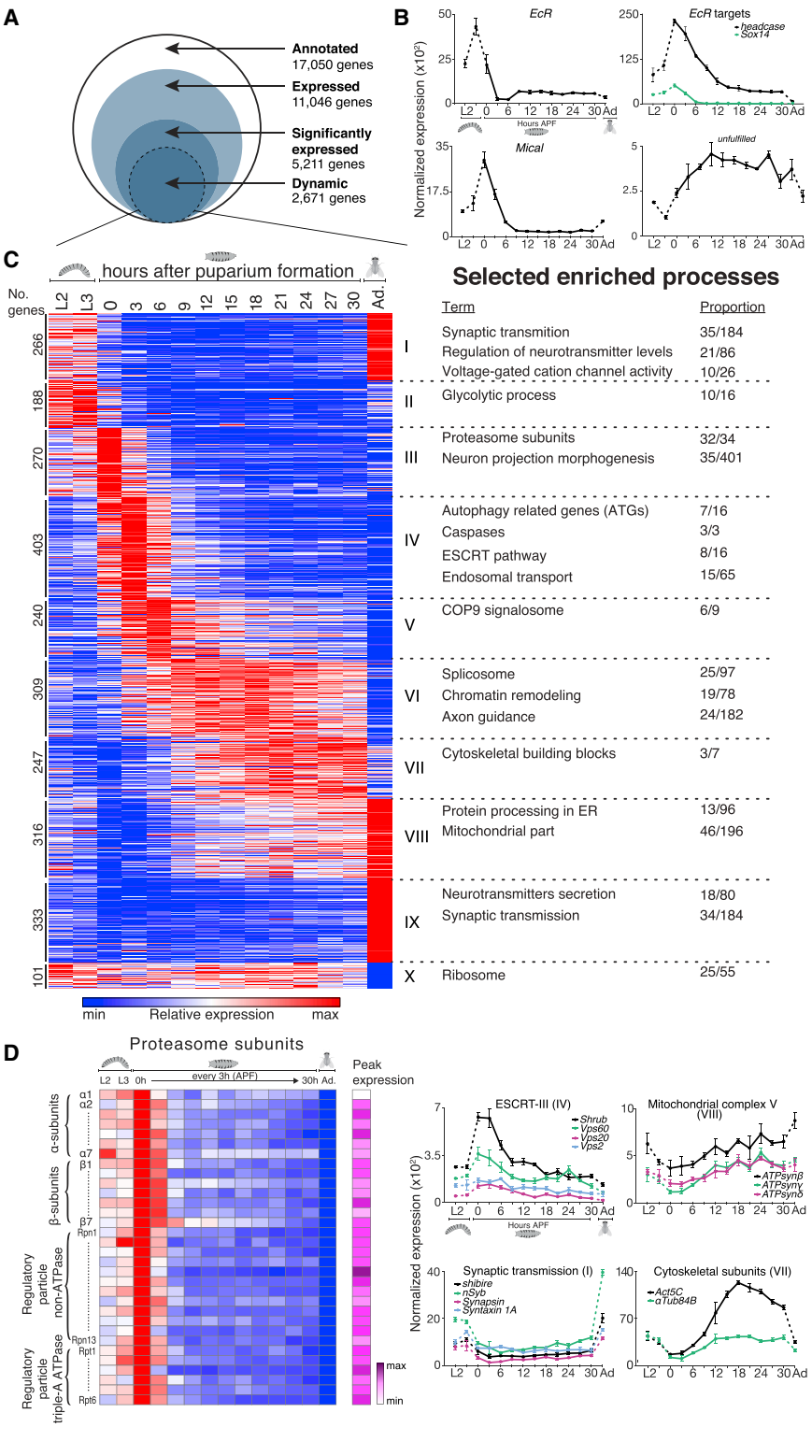

Figure 2. Developmental Expression Atlas Highlights Axon Remodeling Gene Network

(A) Schematic description of the developmental RNA-seq gating analysis. See details in STAR Methods.

(B) Normalized expression of key remodeling related genes across γ neuron development (x axis, only every second time point is labeled due to space limitations; Ad, Adult). Error bars indicate SEM; units on the y axis are arbitrary.

(C) Heatmap showing k-means clustering (k = 10) of 2,671 dynamically expressed genes across MB γ neuron development. Each horizontal line describes the relative expression of a single gene. Cluster numbers are indicated using Roman numerals. Selected enriched processes within each cluster are described on the right (for a full analysis, see Tables S2 and S3). Enrichment is described here as the proportion of genes within the cluster/total number of genes belonging to the functional group and that are significantly expressed.

(D) Examples of functional groups of genes that are expressed in a similar, and interesting, pattern. Heatmap depicting the relative expression patterns of the proteasome subunits (left). The magenta scale depicts the peak expression of each gene relative to that of other genes in the group. Graphs showing the normalized expression levels of selected genes and gene groups throughout development (x axis, every second time point is labeled due to space limitations; Ad, Adult). Error bars indicate SEM; units on the y axis are arbitrary. Cluster numbers are indicated in parenthesis using Roman numerals.

genes from two other degenerative pathways—caspases and autophagy (Figure 2C; Table S2). In contrast to the ESCRT complexes, specific perturbations of the autophagy machinery have so far failed to result in remodeling defects (Issman-Zecharya and Schuldiner, 2014 and data not shown). Interestingly, while caspases have been implicated in dendrite remodeling of sensory da neurons (Schoenmann et al., 2010; Kuo et al., 2006; Williams et al., 2006) as well as in nutrient deprivation remodeling of mammalian neurons (Cosker et al., 2013; Schoenmann et al., 2010), evidence for the involvement of the apoptotic machinery in MB γ remodeling is so far lacking (O.S., unpublished data and Awasaki et al., 2006; Watts et al., 2003). The fact that all of these biological processes are upregulated around the same time, in a seemingly coordinated fashion, suggests that they could act redundantly, eliminating the possibility to visualize a phenotype from simple perturbations to these systems. How these pathways together contribute to various aspects of remodeling remains to be discovered.

Another noteworthy example is the expression profile of synaptic transmission genes that are significantly enriched in clusters I and IX (Figures 2C and 2D; Table S2), exhibiting high expression at larval and adult stages. Whether this dynamic expression is a result of an expected general decrease in

neuronal activity during metamorphosis or rather embeds important neuron-neuron signaling is an interesting avenue for future studies.

One fundamental aspect of MB remodeling is that the γ neurons shift from a degenerative to a regenerative state within a very short time frame as pruning occurs between 6–18 hr APF and by 24 hr APF the same neurons have begun to undergo regrowth. Recently, we found that nitric oxide (NO) signaling provides a switching mechanism between these states, with high NO required for pruning but low NO levels required for the initiation of regrowth. The drastic change in NO levels is achieved, at least in part, by alternative splicing of short isoforms of the NO synthase gene that function as dominant negatives and inhibit the activity of the full-length isoforms (Rabinovich et al., 2016). Interestingly, we found that the spliceosomal complex genes were significantly enriched in cluster VI (Figures 2C and S3B; Table S2). The expression of genes in this cluster gradual increases in the first few hours APF and includes the regrowth-related gene *UNF*, as well as genes related to axon guidance, axon development, and microtubule-associated complexes (Tables S2 and S3). Thus, the enrichment in the spliceosome genes in this cluster hints that a shift in splicing might correlate with the developmental switch from pruning to regrowth. Furthermore, major cytoskeletal components such as the main cytoplasmic actin gene, *Act5C*, as well as the most abundant α and β-tubulin subunits encoding genes, α-Tub84B and β-tub56D, assigned in cluster VII, exhibited a dynamic expression pattern (Figures 2C and 2D; Table S2) that might reflect the switch between the pruning and regrowth.

Finally, we identified a significant enrichment in mitochondrial genes in cluster VIII (Figures 2C and 2D and S3C; Table S2), which contains genes with a specific decreased expression before pruning, followed by increased expression before and during regrowth. This dynamic expression pattern might indicate that mitochondria transcription is a part of the aforementioned cellular switch. Whether this expression transformation is a result of different energy needs or a more instructive mechanism should be further investigated.

Taken together, our high-resolution temporal expression profiling has allowed us to detect the dynamics of gene modules relevant to the different phases of neuronal remodeling. This resource, which can be freely accessed and explored in its entirety (http://www.weizmann.ac.il/mcb/Schuldiner/resources), offers a unique platform to study the development of MB γ neurons and more general timed and stereotypical developmental processes. As such, it highlights specific candidate pathways and genes important during development and suggests possible redundancies and pleiotropies that are otherwise overlooked using conventional genetic tools.

Expression Dynamics of DNA Binding Protein Uncovers New Genes Required for Remodeling

The existence of many dynamic gene modules during γ neuron development suggests that a multi-layered transcriptional network underlies this process. Therefore, we decided to investigate the regulatory factors that govern this network and focused on 177 genes that contain DNA binding domains and are dynamically expressed in our dataset (Table S4; Figure 3A). We chose to focus on the highest expressing DBPs (Figure S4A) within the pruning (II–IV) and regrowth (VI) related clusters (20 genes from each group; we focused on cluster VI for regrowth as it contains the earlier expressed genes which are more likely to function as regulators). In addition, we chose six genes from clusters VII and VIII, which are specifically and significantly ($p < 0.01$) repressed at the onset of pruning (Figures 3A and S4A; for details, see STAR Methods).

To investigate the potential roles of these 46 DBPs in neuronal remodeling, we expressed RNAi or overexpression transgenes targeting each of the up- or downregulated genes accordingly, driven by the MB γ neuron specific driver 71G10. We found that 10 out of these 46 DBPs were involved in neuronal remodeling (Figure 3B), out of which 6 were not previously described in this process. While adult WT MB γ neurons project only to the adult specific medial γ lobe (Figures 3C and 3J), knocking down the expression of *EcR*, *taiman* (*tai*), *maternal gene required for meiosis* (*mamo*), *E75*, *Sox14*, and chronologically inappropriate morphogenesis (*chinmo*) resulted in dorsally projecting γ neurons, indicative of a pruning defect (Figures S4B1–S4H1). In order to validate the RNAi findings, we tested available mutants or generated CRISPR-mediated mutants (Figure S6A) and examined adult brains using the mosaic analysis with a repressible cell marker (MARCM) technique (Lee and Luo, 1999; Figures 3D–3I). Furthermore, overexpression of *Blimp-1*, *HMG protein Z* (*HmgZ*), or *prospero* (*pros*) similarly resulted in unpruned γ neurons (Figures 3K–3M). Since all of these perturbations exhibit normal axon development at the 3rd instar larval stage (Figures S4B2–S4H2 and S4J1–S4L1), while exhibiting unpruned axons at 18 hr APF (Figures S4B3–S4H3 and S4J2–S4L2), the peak of axon pruning, our findings suggest that they are specifically required for remodeling. We verified the protein expression dynamics of selected DBPs and verified their specific elevation during the onset of remodeling (Figures S5A–S5D). This does not rule out, however, other roles for these genes during the development or function of γ or other neurons—in the case of mamo, for example, it is clearly additionally expressed in non-γ cells (Figure S5C). Remarkably, four out of the six most highly expressed genes in the pruning-oriented clusters were found to regulate pruning (*Mamo*, *E75*, *Sox14*, and *EcR*; Figure S3A), out of which three are part of the ecdysone signaling pathway.

Additionally, knocking down *mamo*, *E75,* and *UNF* resulted in incomplete growth of the adult γ medial lobe, indicative of a regrowth defect (Figures S4F1 and S4H1–S4I1). *mamo* MARCM clones indeed exhibit a regrowth defect similar to the RNAi experiments (Figure 3E). Knocking down these genes did not affect initial axon development (Figures S4F2 and S4H2–S4I2).

The TF *Sox14* is a known EcR target and has been shown to regulate dendrite pruning of the sensory da neurons (Kirilly et al., 2009). Previous work on Sox14 has shown that, while RNAi expression within MB neurons resulted in aberrant axon pruning at 24 hr APF (Kirilly et al., 2009), pruning occurred normally in $Sox14^{\Delta 15}$ mutant clones (O.S., unpublished data). However, our newly generated $Sox14^{CRISPR\Delta 1}$ MARCM MB neuroblast clones displayed a clear axon pruning defect (Figure 3F; n = 24/24). Since both of the previously used mutants (Kirilly et al., 2009) contain a small deletion within the first exon, while our mutation is a full deletion of the gene, one potential explanation of this discrepancy is the existence of an alternative start site that might be differentially expressed between the da and MB neurons.

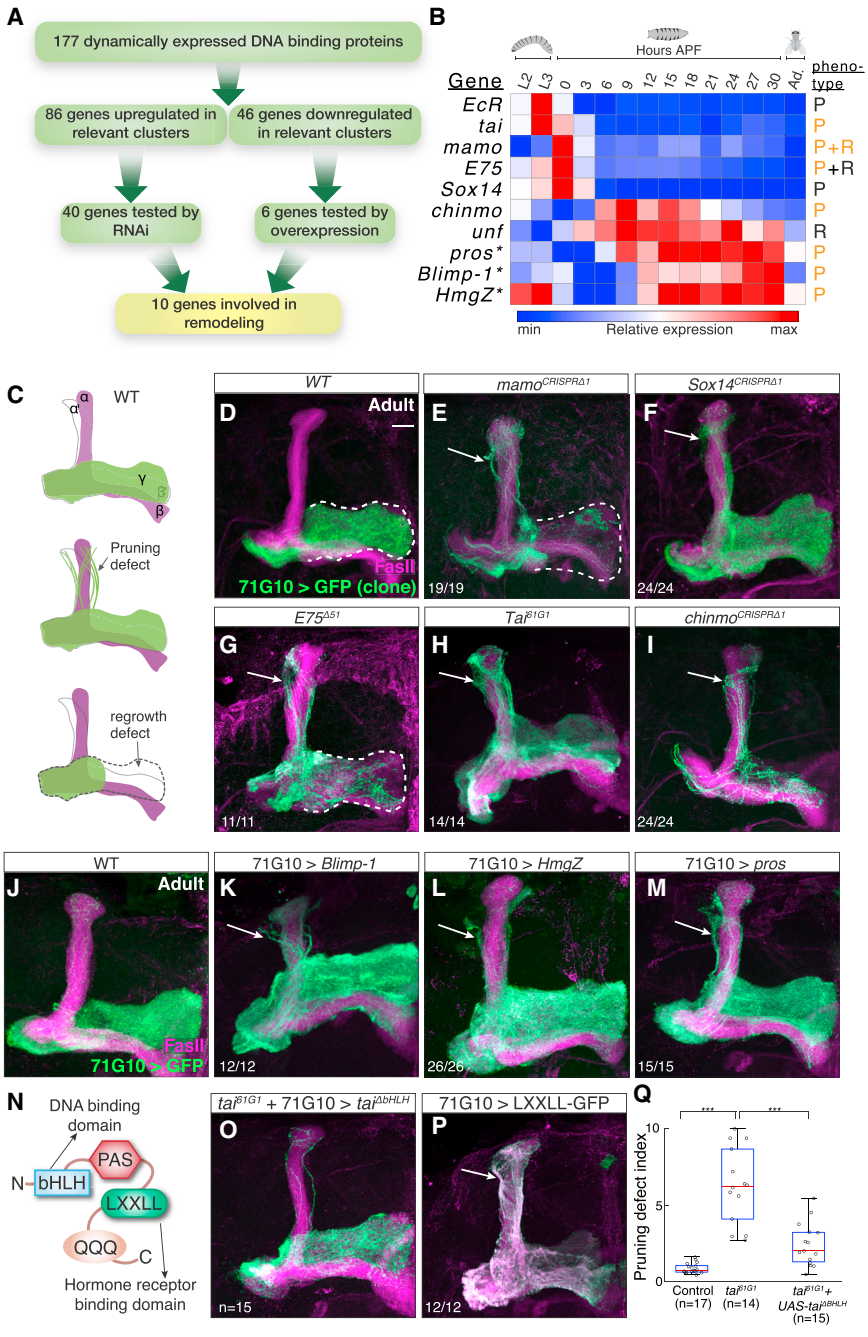

Figure 3. Dynamic Expression of DNA Binding Proteins Highlight New Genes Required for Remodeling

(A) Scheme of the rationale for the DNA binding protein screen, including the number of genes in each step.

(B) Heatmap showing the relative expression pattern of the 10 positive hits in the DNA binding protein screen. The expression patterns of all 46 genes experimentally tested are shown in Figure S3. Genes were perturbed by RNAi or overexpression (asterisk) experiments. P and R stand for pruning or regrowth phenotypes, respectively. While genes known to be required for remodeling are labeled in black, new findings from this study are labeled in orange.

(C) Schematic representation of WT and defective MBs depicting pruning and regrowth defects. Green represents the γ lobe(s) and magenta represents FasII staining, which in the adult strongly labels α/β neurons, weakly labels γ neurons (not shown for clarity), and does not label α′/β′ neurons.

(D–I) Confocal Z-projections of adult MBs containing WT (D), *mamo*$^{CRISPR\Delta1}$ (E), *Sox14*$^{CRISPR\Delta1}$ (F), *E75*$^{\Delta51}$ (G), *Tai*^{61G1} (H), and *chinmo*$^{CRISPR\Delta1}$ (I) MARCM clones labeled with membrane bound mCD8-GFP (GFP) driven by 71G10-GAL4 (71G10).

(J–M) Confocal Z-projections of adult MBs labeled by 71G10-Gal4 driven mCD8-GFP (GFP) additionally expressing *Blimp-1* (K), *HmgZ* (L), and *pros* (M).

(N) Schematic diagram of Tai depicting the basic-helix-loop-helix (bHLH) domain required for DNA binding, the LXXLL domain required for binding hormone receptors, the PAS domain, and the poly Q activation domain.

(O) Confocal Z-projections of adult *tai*^{61G1} MB MARCM neuroblast clones labeled by 71G10-Gal4 driven mCD8-GFP additionally expressing a *tai* rescue transgene lacking its bHLH domain (ΔbHLH).

(P) Confocal Z-projection of an adult MB with 71G10-Gal4 driving the expression of mCD8-GFP and as well as the hormone receptor binding domain of Tai fused to GFP.

(Q) Quantification of the pruning severity in (D), (H), and (O). We automatically designated a pruning index to each brain based on image analysis (see STAR Methods). Box centers indicate the median, and the bottom and top edges indicate the 25th and 75th percentiles, respectively. The whiskers extend to the most extreme data points not considered outliers (99.3% coverage if the data is normally distributed). ***p < 0.001; see Figure S6B for a parallel, blind ranking quantification.

Pruning defects, evident by dorsally projecting γ neurons, are marked by arrows, while a regrowth defect, evident by incomplete innervation of the adult γ lobe, is demarcated by a white dashed line. Green is mCD8-GFP driven by 71G10-Gal4; magenta is FasII staining; scale bar represents 15 μm. The numbers (x/n) on the lower left corners depict the number of times the phenotype was observed out of the total hemispheres examined.

E75 is another well-described target of EcR that we have previously shown to be involved mainly in axon regrowth following pruning (Rabinovich et al., 2016; Figure 3G). While the previously published allele, *E75*$^{\Delta51}$, also displays a moderate pruning defect (Rabinovich et al., 2016; Figure 3G), the notable high expression of E75 at the onset of pupation compared to later stages suggested a more significant role in the pruning process. Indeed, knocking down E75 using RNAi resulted in a significant pruning defect (Figure S4H1). Since *E75*$^{\Delta51}$ contains a deletion of only part of the gene and is proposed to perturb some but not all isoforms, one possible explanation is that different isoforms might be differentially required for pruning and regrowth.

tai is an ortholog of the mammalian NR coactivator 3, which is part of the family of steroid receptor coactivators (SRCs). It

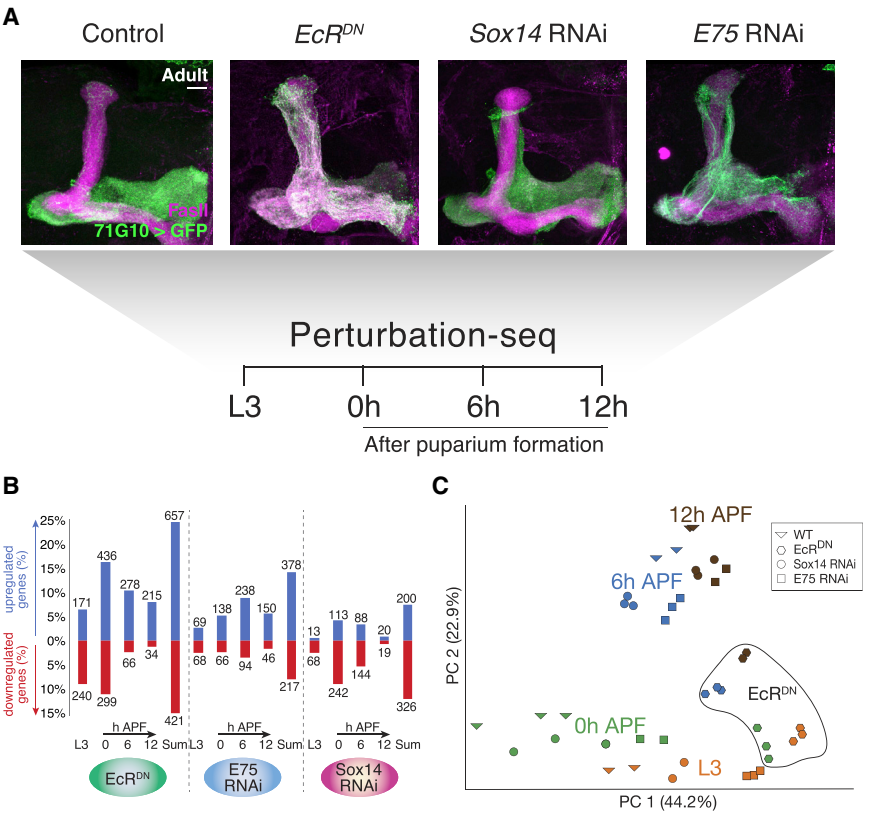

Figure 4. EcR Mediates Larval to Pupal Transition as Identified by Perturbation Sequencing

(A) Schematic overview of the genotypes and time points taken for perturbation sequencing. The images are confocal Z-projections of adult MB γ neurons labeled with mCD8-GFP (GFP) driven by 71G10-GAL4 (71G10) additionally expressing the indicated transgenes and counterstained with FasII antibody (magenta). Scale bar represents 15 μm.

(B) Quantification showing the number of genes affected by each TF perturbation at each developmental time point as compared to WT.

(C) Principal-component analysis (PCA) of the expression profiles of WT and perturbed MB γ neurons throughout development. Colors demarcate the developmental time, while the shape of each icon represents its genotype.

contains a basic-helix-loop-helix (bHLH) domain that allows it to bind DNA directly, as well as an LXXLL domain that mediates binding to the hormone-bound NR (Figure 3N; Bai et al., 2000). Previous studies have implicated *tai* in border cell migration in the *Drosophila* ovary, functioning together with *EcR* and its co-receptor *usp* (Jang et al., 2009; Bai et al., 2000). However, the function of *tai* in other tissues has not been thoroughly examined. Knockdown of *tai* expression using RNAi resulted in a mild pruning defect (Figure S4D1). However, MB neuroblast MARCM clones homozygous for tai^{61G1}, an established EMS loss-of-function mutant, exhibit a severe defect (Figure 3H; n = 14/14), suggesting that the weak RNAi phenotype might be due to the variable efficiency of the RNAi strategy in neurons. We further confirmed the Tai protein expression pattern, which revealed high expression levels in MB γ neurons at 0 hr APF (data not shown) congruent with EcR-B1 (Lee et al., 2000). Tai can potentially function as an independent TF (thus requiring its bHLH DNA binding domain), or as a coactivator of NRs. To investigate the requirement of the bHLH domain in axon pruning, we performed a rescue experiment by expressing a *tai* transgene lacking this domain ($tai^{\Delta bHLH}$) within a tai^{61G1} MARCM clone. We found that expression of $tai^{\Delta bHLH}$ was sufficient to rescue the tai^{61G1} pruning defect (Figure 3O; quantification in Figures 3Q and S6B; n = 15), suggesting that the DNA binding domain of Tai is dispensable for its function in this context. However, overexpression of Tai's hormone receptor binding domain (LXXLL) fused to GFP in WT clones was sufficient to cause a severe pruning defect (Figure 3P; n = 12/12), supporting its reported dominant negative function, most likely by sequestering EcR (Jang et al., 2009). In order to further examine the role of *tai* as a member of the EcR NR complex, we tested whether mutating *tai* affects the expression levels of known EcR targets such as *Sox14* and *E75*. Indeed, we found that tai^{61G1} MB neuroblast MARCM clones exhibit significant lower Sox14 protein levels (Figure S6C). Since a good E75 antibody has yet to be generated, we instead examined the antibody staining of Mamo, which we found to be regulated by E75 (Figures S7C and S7L). As expected, Mamo staining was drastically decreased in *tai* mutant clones (Figure S6D), suggesting that Tai positively regulates the EcR targets and is consistent with it functioning as a coactivator for the EcR/Usp NR complex.

Our data-driven mini-RNAi screen yielded many factors required for pruning but, in contrast, identified fewer DBPs required for regrowth. One possible explanation is that the regulation of developmental regrowth is less complex than that of pruning or that it involves mostly post-transcriptional regulation, such as alternative splicing. Alternatively, the difference might be inherent to the phenotypes since identifying a pruning defect involves visualization of ectopic axons that do not normally exist, and thus even a minor defect is relatively easy to detect. In contrast, assaying for a regrowth defect requires many axons to be defective at the same time, as they project together to the medial lobe and a minor defect in some but not many of the axons might be masked.

Our results demonstrate the power of developmental expression profiling as a tool for finding new regulators of a complex developmental program such as neuronal remodeling. Additionally, our data suggest that the transcriptional regulation of remodeling is much more complex than previously appreciated.

EcR Mediates Larval to Pupal Transition in a Cell-Autonomous Manner

In order to link between the transcriptional regulators and the developmental modules, we compared the expression profiles

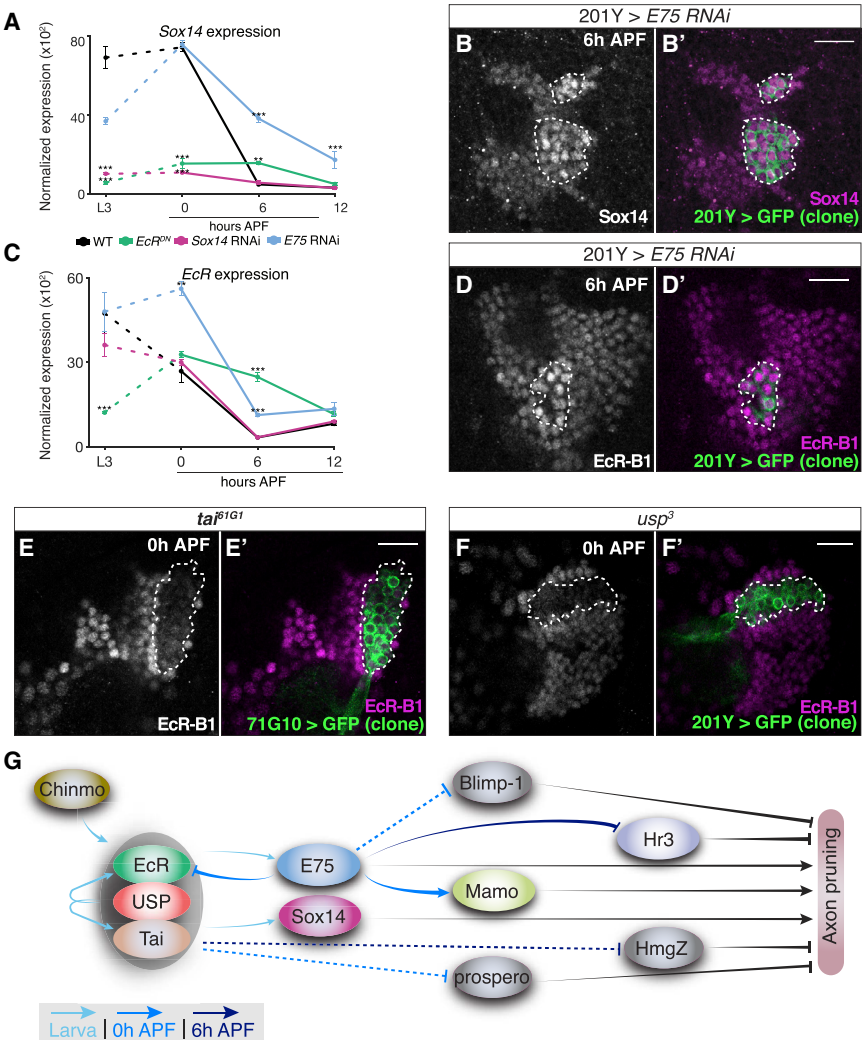

Figure 5. Hierarchical TF Networks Regulate Axon Pruning

(A and C) Normalized expression of Sox14 (A) or EcR (C) in WT MB γ neurons and in those expressing the indicated transgene (**p < 0.01; ***p < 0.001). Error bars indicate SEM; units on the y axis are arbitrary.

(B and D–F) Confocal single slices of the cell body region of MBs containing neuroblast clones labeled with 201Y-GAL4 (B, D, and F) or 71G10-GAL4 (E) driven mCD8-GFP (green), additionally driving the expression of *E75* RNAi (B, n = 5; D, n = 4), or mutant for tai^{61G1} (E, n = 6) or usp^{3} (F, n = 5). Brains are stained with anti-Sox14 (B) or anti-EcR-B1 (D–F) (magenta) at the indicated time points. Clones are demarcated by dashed lines. The Sox14 antibody staining was increased by 2.2-fold (p < 0.001) within clones expressing *E75* RNAi. Expression levels of EcR exhibited a 2.5-fold increase (p < 0.01) within the clone expressing E75 RNAi and a 2.9-fold (p < 0.001) and 3-fold (p < 0.001) decrease within the usp^{3} and tai^{61G1} clones, respectively.

Scale bars represent 15 μm.

(G) Schematic model based on data presented here and in Figure S6, describing the hierarchical regulation of axon pruning by regulatory factors as uncovered in this study. The gray ellipse encompassing EcR, Usp, and Tai represents the NR complex. The temporal dimension is represented by the blue color tones of the arrows. While full lines were validated by antibody expressed experiments, dashed lines indicated regulation interpreted only from the RNA-seq data.

of WT γ neurons and those perturbed for key TFs required for axon pruning: EcR, Sox14, or E75. To this end, we expressed a dominant negative form of EcR (EcR^{DN}), Sox14 RNAi, or E75 RNAi within γ neurons (see adult phenotypes in Figure 4A) and extracted RNA-seq data at four stages—L3, 0, 6, and 12 hr APF.

On a global view, expression of EcR^{DN} resulted in the most dramatic global transcriptome changes—39% of the genes that were dynamically expressed during development (and hence contained in one of our developmental clusters) exhibited at least 2-fold change of expression, in at least one time point compared to their normal expression (Figure 4B; Table S5). E75 and Sox14 perturbations resulted in significant expression changes of 22% and 19% of the genes, respectively (Figure 4B). PCA (Figure 4C) resulted in a primary axis (PC1) representing the transition from larva to pupa and PC2 correlating with the gradual developmental transition. Strikingly, neurons expressing EcR^{DN} showed a high degree of similarity with WT larval neurons regardless of the developmental stage in which they were dissected. In contrast, neurons that expressed Sox14 or E75 RNAi formed distinct clusters with their biological replicates based on the similarity of their global expression but still exhibited a relatively high degree of similarity with their age-matched WT control. Taken together, these results suggest that EcR is not only the master regulator of neuronal remodeling in multiple neuron types but rather dominates the entire transcriptional transition from larva to pupa in MB neurons in a cell-autonomous manner.

Hierarchical TF Networks Regulate Axon Pruning

Next, we analyzed the expression profiles of WT and perturbed MB γ neurons to uncover the epistatic interactions between *EcR, Sox14*, and *E75*. As expected, RNA levels of *E75* as well as RNA and protein levels of *Sox14*, both of which were shown to be downstream effectors of EcR, were significantly reduced in neurons expressing EcR^{DN} (Figures S7A and S5A and data not shown). However, when we compared the expression levels of *Sox14* in WT neurons to those expressing E75 RNAi, we noticed a dramatic increase in *Sox14* RNA levels at 6 hr APF (Figure 5A), suggesting that *E75* inhibits *Sox14* expression at this developmental time point. This is an unexpected finding since we did not observe significant changes in Sox14 RNA or protein levels at L3 or 0 hr APF in E75 RNAi-expressing cells (Figure 5A and data not shown). Based on the known features of this transcriptional network (Kirilly et al., 2009), we therefore speculated that E75 might affect Sox14 expression via feedback inhibition of EcR. Indeed, while *EcR* expression was not altered by Sox14

RNAi, perturbing E75 resulted in increased EcR expression at 0 hr APF (Figure 5C), suggesting a negative feedback loop. To extend this result from RNA to the protein level, we generated MARCM clones expressing *E75* RNAi and observed an increase in both EcR-B1 and Sox14 antibody staining within the clones compared to the neighboring cells (Figures 5B and 5D).

Our transcriptome analysis also revealed that EcR^{DN} expression caused a reduction of EcR RNA levels at L3 (Figure 5C). EcR^{DN} encodes for a truncated NR, lacking its activation domain (ΔC655.W650A; Cherbas et al., 2003) and is therefore not expected to affect the endogenous transcript level. Rather, this result suggests a positive auto-regulatory loop during early development that we decided to further examine. Indeed, usp^{3} or tai^{61g1} MARCM clones exhibited a drastic decrease in EcR-B1 protein levels at 0 hr APF (Figures 5E and 5F). Together, these results are indeed consistent with a positive auto-regulatory loop between the function of the EcR/Usp/Tai NR complex and the RNA expression levels of EcR-B1. At 6 hr APF, however, we found increased EcR RNA levels within cells expressing EcR^{DN} (Figure 5C), suggesting the existence of a negative feedback at this pupal stage. The parsimonious interpretation that takes into consideration the entire dataset is that expressing EcR^{DN} results in decreased E75 levels (Figure S7A), which in turn release the suppression of EcR later on. In conclusion, our results describe the dynamic and developmentally regulated expression of an EcR regulatory network. We have uncovered two feedback loops—a positive auto-regulatory loop of the *usp-EcR* complex and a negative feedback of *EcR* transcription by E75 (included in the broader model illustrated in Figure 5G).

Finally, we decided to similarly analyze the effect of the three TFs on the DBPs that we identified earlier. Using similar analyses of the RNA-seq expression data, in most cases followed by antibody studies in genetically perturbed conditions (Figures S7A–S7P), we broadened the regulatory-factor hierarchy that orchestrates various aspects of pruning (Figure 5G).

Complex Regulation of TF Circuits Controls Distinct Developmental Programs

Although the TFs are the master coordinators of remodeling, the executioners would be their downstream targets. Thus, we next aimed to better characterize which biological processes are regulated by EcR, Sox14, and E75 that culminate in the execution of neuronal remodeling. This dataset is dimensionally complex as it includes expression profiles of thousands of genes obtained from cells of four different genotypes at four different time points. Therefore, it seems that normal cluster analysis would be difficult to interpret. Instead, we decided to explore the effects of the different TF perturbations on the expression of specific developmental clusters. Our hypothesis was that re-clustering the genes within each developmental cluster, according to their response to a TF perturbation, would highlight specific co-regulated modules (Figure 6A). In other words, we looked for groups of genes within each cluster that are similarly affected by perturbation of EcR, E75, or Sox14. Indeed, the new sub-clusters revealed a unique pattern of temporal regulation by the three key TFs (k = 2–4 sub-clusters for each developmental cluster; Figure 6B; Table S5). The heatmap analysis in Figure 6B is not optimal for two main reasons: first, because it depicts relative expression in contrary to the absolute expression, it may generate a false impression of changes in gene expression. For example, cluster IIIb exhibits a notable increase in expression at 6 hr APF in cells expressing E75 RNAi, resulting in the false impression that its expression does not peak at 0 hr APF in WT cells, as the rest of cluster III. Second, the results from this kind of analysis are not readily quantifiable. Therefore, we looked for a better visualization method that could also allow quantification of the combinatorial effect on each sub-cluster. To this end, we generated boxplots for each sub-cluster representing the effect of each perturbation on the expression of the genes in the sub-cluster (Figures 6C and 7A; Table S5; see details in STAR Methods). In each boxplot, the dashed line represents the average normalized expression trend of the genes within the sub-cluster. In the case of clusters IIIa–c, for example, the dashed line represents the peak expression at 0 hr APF. Note that the dashed line in cluster IIIb still represents a peak at 0 hr APF, unlike the false impression in the heatmap analysis in Figure 6B. The boxplots represent the normalized expression of the genes within the sub-cluster in the appropriate perturbation. For each sub-cluster, we can therefore assign a regulator network, as depicted beside each of the sub-cluster boxplots (Figure 6C). For example, genes within sub-cluster IIIa are mostly inhibited by EcR^{DN} at L3 and 0 hr APF but are unaffected by perturbation of *Sox14* and *E75*, suggesting that sub-cluster IIIa is positively regulated by EcR, either directly or indirectly via an unknown target. In contrast, clusters IIIb and IIc are positively regulated by EcR and Sox14, while cluster IIIb is also negatively regulated at later time points by E75. Delving further into cluster IIIa, we decided to explore whether genes within this cluster were directly regulated by EcR. While the conclusive approach here would be to perform ChIP-seq analyses, these are time consuming and extremely challenging, given the small number of cells in our samples. Therefore, in order to discriminate between direct and indirect regulation of sub-cluster IIIa by EcR, we performed Spearman correlation analysis of the sub-cluster weighted expression and *EcR* expression. Since we expect a delay between EcR mRNA expression and the mRNA expression of its targets, we performed the analysis between EcR expression and the sub-cluster weighted expression in the next time point available, which was (t) = 6 hr post each time point (for example, EcR expression at 0 hr APF compared to the sub-cluster weighted expression at 6 hr APF; details in STAR Methods). While the Spearman correlation score without delay was $r_s = 0.05$, the correlation score with the delay was $r_s = 0.88$, suggesting a potentially direct induction of sub-cluster IIIa by EcR. This sub-cluster contains 64 genes that include most of the common proteasome subunits (29 genes out of the 32 that exist in cluster III; Figure 6D; and Tables S5 and S6). Taken together, these results suggest that the proteasome subunits as well as the entire IIIa sub-cluster are directly regulated by EcR but not by Sox14 or E75.

Our genome-wide perturbation analyses suggest that sub-clusters IVa and IVb (which contain 125 and 100 genes, respectively; Figure 7A) are both positively regulated by EcR as well as Sox14. Sub-cluster IVa contains most of the autophagy-related genes (ATGs) included in developmental cluster IV and 4 out the 8 ESCRT genes included in this cluster. It is also enriched with genes belonging to the endosome compartment (GO:0005768;

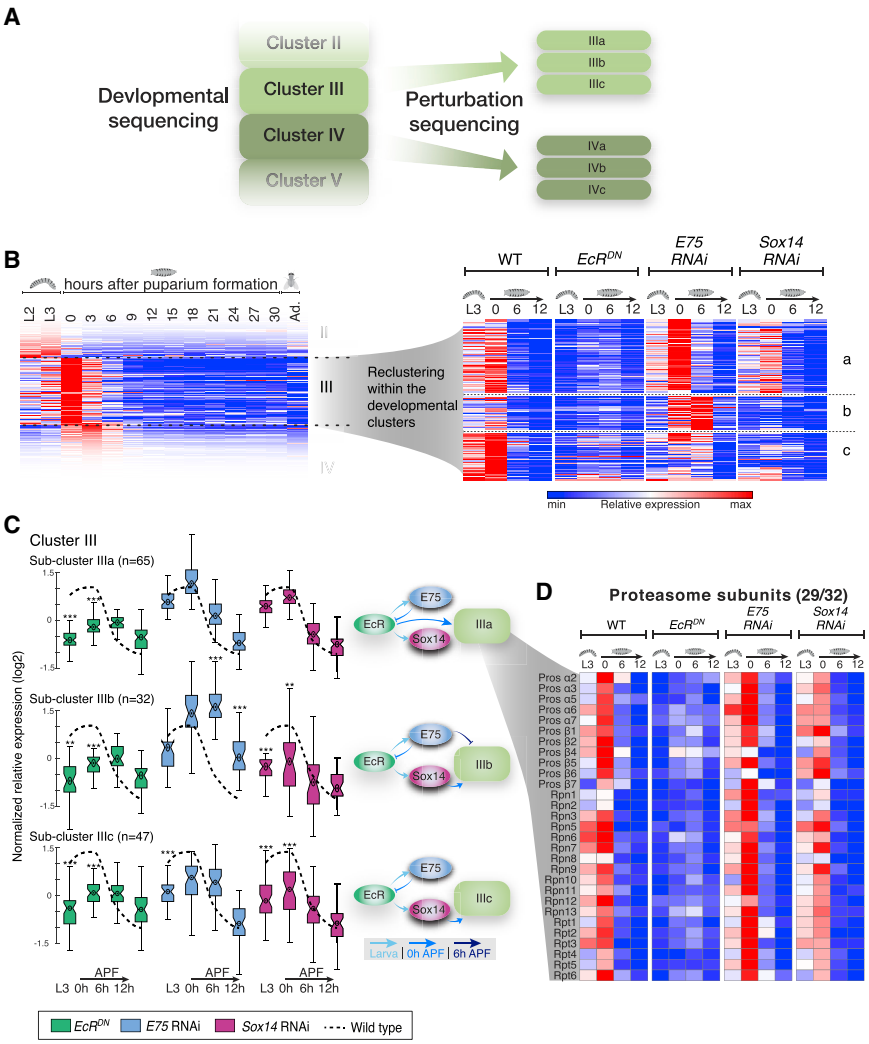

Figure 6. Combining Developmental Clustering with Perturbation Sequencing Is a Powerful Strategy to Reveal Functional Groups of Genes Co-regulated by TF Modules

(A) Schematic representation of the sub-cluster analysis. Each developmental cluster was further divided into sub-clusters with a unique pattern of response to the TF perturbations (by k-means clustering; k = 2–4 for each cluster). The sub-clusters contain only genes whose expression significantly changed in at least one perturbation (see STAR Methods for more information).

(B) Heatmaps of developmental cluster III (left) and the three sub-clusters IIIa–c in the perturbation-seq (right) as an example. Similar analyses were conducted for all developmental clusters (see Table S5).

(C) Boxplot analyses of sub-clusters IIIa–c. The average normalized relative gene expression of the WT samples within each sub-cluster is depicted by the dashed line. Boxplots of the normalized relative gene expression for each one of the perturbations in each time point are shown. Box centers indicate the median, and the bottom and top edges indicate the 25th and 75th percentiles, respectively. The whiskers extend to the most extreme data points not considered outliers (99.3% coverage if the data are normally distributed). Statistical significance was determined (**$p < 0.01$; ***$p < 0.001$; see STAR Methods) but shown only in cases where the average fold change >2 and thus more likely to also be biologically significant. The hierarchal regulation of each sub-cluster, as inferred from the data, is presented schematically where the temporal dimension is represented by the shades of blue of the arrows.

(D) Heatmap depicting the relative expression patterns of the proteasome subunits, belonging to cluster IIIa, in the different perturbations. Number (x/y) represent the number of genes from the functional group within the sub-cluster (x) / the number of genes from the functional group within the parent cluster (y).

Figure 7A; Table S6). Sub-cluster IVb is enriched with genes related to the positive regulation of the apoptotic signaling pathway (GO:2001235) and contains all 3 caspases that are significantly expressed in γ neurons. Our analysis further showed high correlation between the two sub-clusters' expression pattern and the delayed expression of *Sox14* but not of *EcR* or *E75*, (r_s = 0.84, 0.72, and 0.62 for sub-cluster IVa; and r_s = 0.81, 0.45, and 0.46 for sub-cluster IVb, respectively), suggesting that genes in both sub-clusters may be directly regulated by Sox14. Thus, together, clusters IVa and IVb represent two gene modules that are likely directly regulated by Sox14 and are enriched with proteins belonging to several degradative pathways—endosome-related genes, the ESCRT complex, autophagy, and apoptosis. Finally, cluster VIIIa, containing 122 genes, is substantially enriched with genes belonging to three KEGG or GO terms: the citric acid cycle (TCA, map00020), aerobic respiration (GO: 0009060), and mitochondria (GO: 0044429). This sub-cluster seems to be specifically inhibited by EcR, perhaps by direct regulation (Table S5; Spearman correlation $r_s = -0.76$). Whether the downregulation of genes within this cluster is a causal driver of axon pruning requires further investigation.

To conclude, clustering of differentially expressed genes based on their normal developmental expression, followed by sub-clustering of these developmental modules based on their response to specific perturbations to key TFs, enabled us to identify sub-clusters and groups of functionally related genes that are specifically regulated by a set of TF combinations as a function of developmental time. We have focused here on some example clusters, but the full dataset is available and analyzed in Tables S5 and S6 and is directly approachable in its entirety via http://www.weizmann.ac.il/mcb/Schuldiner/resources.

Overall, our perturbation-seq analysis on the basis of the developmental sequencing results in a temporal map of biological processes that are induced or repressed by unique transcriptional circuits during γ neuron development. Some of these functional groups are already known to be required for distinct steps in neuronal remodeling, and in addition, our analysis highlighted new genes and pathways whose coordinated regulation

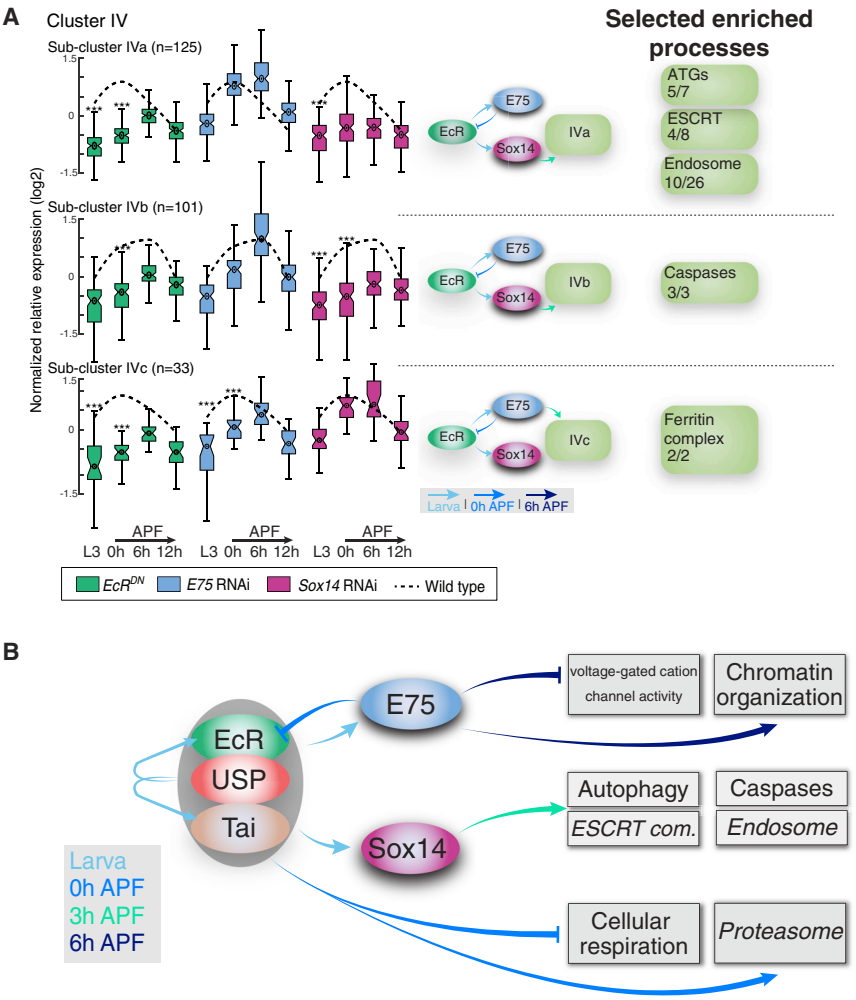

Figure 7. Toward a Temporal Understanding of the Expression Landscape that Underlies Neuronal Remodeling of MB γ Neurons

(A) Boxplot analyses of sub-clusters IVa–c. The average normalized relative gene expression of the WT samples is depicted by the dashed line. Boxplots of the normalized relative gene expression for each one of the perturbations in each time point are shown. Box centers indicate the median, and the bottom and top edges indicate the 25th and 75th percentiles, respetively. The whiskers extend to the most extreme data points not considered as outleirs (99.3% coverage if the data is noramlly distributed). Statistical significance was determined (***p < 0.001; see STAR Methods) but only shown in cases where the average fold change >2 and thus more likely to also be biologically significant. The hierarchal regulation of each sub-cluster, as inferred from the data, is presented schematically where the temporal dimension is represented by the shades of blue of the arrows. On the right, we label selected groups of genes that are functionally related and enriched within the sub-cluster. Numbers (x/y) represent the number of genes from the functional group within the sub-cluster / the number of genes from the functional group within the parent cluster.

(B) A schematic model based on data presented and analyzed in Figures 6 and 7 and Table S5, describing the temporal regulation or specific transcription modules by the indicated TFs. GO terms with genes that have a known function in remodeling are highlighted in italics. The temporal dimension is represented by the color of the arrows.

might be required for remodeling and that might not have been easily identifiable using current genetic approaches (Figure 7B). More generally, it provides a broad map of the immense transcriptional effort that must be carried out to enable such a dramatic developmental program as elimination of cellular parts and their subsequent re-creation.

DISCUSSION

Gene Expression Is Highly Dynamic during Development

During the last decade, several studies have conducted wide transcriptional analyses of cell populations or tissues *in vivo* during development (Ren et al., 2017; Shigeoka et al., 2016; Liu et al., 2015; Molyneaux et al., 2015), but the temporal resolution was normally limited to 3 or 4 time points and included few samples per tissue. A recent study sequenced 9 developmental stages to discover discrete transcriptional phases during microglia development, thus demonstrating the power of higher temporal resolution (Matcovitch-Natan et al., 2016). However, due to the nature of the developmental process studied, the temporal gap between the stages was rather large (days). In the present study, we performed developmental sequencing in an unprecedented temporal resolution that enabled us to fully capture the neuronal remodeling program, which takes place during a very short time frame. As seen by the global correlation analysis, expression patterns are extremely dynamic even in a 3-hr window, especially during early metamorphosis. While studies have previously shown expression dynamics in these timescales of key TFs during development (Truman et al., 1994; Klingler and Gergen, 1993; Biggin and Tjian, 1989), the finding that these rapid changes occur on a global level is remarkable. While this paper was in revision, three papers dissected the early steps of zebrafish embryogenesis, further demonstrating the power of our strategy (Briggs et al., 2018; Farrell et al., 2018; Wagner et al., 2018).

Complex Feedback Loops Regulate the EcR Signaling Pathway

The TF hierarchy that we identified uncovered a multilayered regulatory network that governs pruning. Specifically, we identified positive and negative feedback loops on EcR transcription. Our study also indicates the domination of EcR signaling on the entire transcriptional transition from larva to pupa in MB neurons in a cell-autonomous manner. Therefore, it is reasonable to speculate that other layers of regulation will support EcR signaling tuning. Boulanger et al. (2011) showed that *ftz-f1* and *Hr39* function

upstream of *EcR* in MB γ neurons, with *Hr39* suggested to act as an inhibitor of EcR. King-Jones and Thummel (2005), however, suggested that Hr39 is a downstream target of EcR. Our expression analyses indicate that the expression of *Hr39* in γ neurons peaks at 0 hr APF (cluster III; Figure S4A), which lags after the EcR peak itself. Furthermore, Hr39 expression is dramatically reduced in samples expressing EcR-DN (not shown), consistent with Hr39 being a bona fide downstream target of EcR as previously suggested (King-Jones and Thummel, 2005). A hypothesis that combines these seemingly contradictory findings is that EcR and Hr39 form a negative feedback loop, just like the one we discovered here between EcR and E75. The complex feedback regulation on EcR expression suggests its precise expression levels and temporal regulation are crucial for normal development. The combined existence of positive as well as negative feedback loops to regulate key developmental or homeostatic processes, such as muscle differentiation (Potthoff and Olson, 2007) and the circadian clock (Barkai and Leibler, 2000), suggests that this is a common evolutionary strategy to confer expression robustness in noisy conditions.

Combining Developmental-Seq and Perturbation-Seq Is a Powerful Strategy to Uncover Developmental Programs

Several studies have sequenced normal as well as mutant cells (Dixit et al., 2016; Jaitin et al., 2016; Hoopfer et al., 2008), which led to significant findings regarding the transcriptional changes resulting from these perturbations. In the present study, however, we combine the fine developmental expression atlas with the expression profiles of neurons perturbed in three key TFs at four developmental stages. This resolution not only facilitates identifying the putative direct and indirect targets of these TFs but also highlights the temporal and hierarchical dynamics of their regulation. Each one of these TFs has hundreds to thousands of potential targets. Thus, a normal candidate approach would have been time demanding and inefficient. By integrating the perturbation-seq data into developmental-seq clusters, we identified groups of genes that were developmentally co-regulated by a unique TF combination, which in turn assisted us to construct the chronological regulation of varied transcriptional programs during γ neuron development. In conclusion, this strategy is powerful in identifying the dynamics of important developmental programs using rich expression profile data.

The approach that we have demonstrated here should be useful to dissect other complex developmental programs. The two prerequisites are that the studied cells can be labeled and purified and, in addition, that one or more TFs are either known to regulate the development of the cell type studied or identified within the process. Most obviously, with the temporal-developmental expression atlas that we have built for MB γ neurons, one could focus on developmental axon regrowth and the TF network so far comprising UNF and E75. Additionally, we and others have previously shown that astrocyte-like glia are required for different aspects of MB neuronal remodeling and depend on cell-autonomous expression of EcR (Hakim et al., 2014; Tasdemir-Yilmaz and Freeman, 2014). Finally, this strategy could be useful to study mammalian developmental programs, such as bone or cartilage development where identifiable groups of cells were shown and various TFs demonstrated to be required for the developmental process. For example, chondrocyte development is tightly regulated by a complex transcriptional network including various SOX-family as well as Runx family TFs that execute the transition from immature to hypertrophic chondrocytes (Kozhemyakina et al., 2015). One aspect that should be specifically tailored for each system is the temporal resolution, which is likely to be longer gaps in mammals.

The Detailed Transcriptional Landscape of MB γ Neurons Holds the Promise to Uncover Parallel and Presumably Redundant Pathways

In the context of the neuronal remodeling field, the dramatic and overarching transcriptional dynamics that we have uncovered here is, in our opinion, surprising. Studies in the recent two decades highlighted signaling between glia and neurons via the TGF-β pathway as a key trigger of neuronal EcR signaling, which is required to initiate axon pruning (Yu and Schuldiner, 2014). The role of adhesion and cytoskeletal stability was also known and thus transcriptional dynamics of related genes expected. Nonetheless, in our study, we found that 51% of the genes significantly expressed in MB γ neurons exhibited dynamic expression within the time frame of neuronal remodeling. These global changes suggest that the developmental remodeling might involve a more complex program than we initially anticipated.

The detailed expression profiles that we have extracted from MB γ neurons throughout development provide a unique opportunity to uncover parallel and redundant pathways. The example of *hdc* and *Mical*, targets of *EcR* and *Sox14*, respectively, is discussed above. Similarly, Spastin was recently shown to be required for branch-specific pruning at the mammalian neuromuscular junction (NMJ) (Brill et al., 2016). Despite its highly relevant expression (peak at 0 hr APF; 3.3-fold increase from L3), we did not observe a pruning defect in *spastin* mutants (data not shown), suggesting that parallel mechanisms might mask its function. More experiments are needed to uncover the detailed MT dynamics as well as the combined function of different MT regulators during pruning.

Finally, caspases were shown to be required for proper pruning in *Drosophila* da neurons (Schoenmann et al., 2010; Kuo et al., 2006; Williams et al., 2006) as well as axon elimination of mammalian dorsal root ganglion (DRG) neurons following trophic deprivation *in vitro* (Simon et al., 2012; Schoenmann et al., 2010) and pruning of mouse retinocollicular connections *in vivo* (Simon et al., 2012). Our RNA-seq data highlight a regulatory module, positively regulated by Sox14 at the early pupal stage, which includes three degradative pathways—the apoptotic machinery (mostly caspases), the autophagic pathway, as well as the endocytic machinery (clusters IVa and IVb). We and others have previously demonstrated that the endocytic machinery is required for pruning of MB axons and *da* dendrites (Loncle et al., 2015; Issman-Zecharya and Schuldiner, 2014; Zhang et al., 2014), but a role of caspases and the autophagic machinery in MB neuron pruning is still lacking (Watts et al., 2003 and data not shown). Our data highlight a potential cross-talk between these degradative pathways, which should be further explored in multiple model systems. Interestingly, the defects in retinocollicular refinement when caspases are inhibited are only partial,

suggesting that redundant mechanisms might also be important in mammalian systems.

To conclude, we demonstrate here the power of detailed developmental sequencing combined with a genetically tractable system. We have identified here a complex network of regulatory proteins that control different aspects of neuronal remodeling. The eleven DBPs that are described here, most of which (9/11) have predicted conserved mammalian orthologs, should form a good pool of candidate genes that could also be tested in vertebrates, where the understanding of the transcriptional regulation of remodeling is scarce. The entire dataset could serve as a valuable resource for groups studying MB neurons as well as neurodevelopment in general. In the future, it should be compared to other temporal-developmental expression datasets extracted from other neurons in vertebrates and invertebrates. Most importantly, the strategy to combine detailed developmental sequencing with sequencing of perturbed neurons, which we used here to describe the temporal regulation of specific genetic modules, could be used to dissect other developmental programs across the animal kingdom.

STAR★METHODS

Detailed methods are provided in the online version of this paper and include the following:

- KEY RESOURCES TABLE
- CONTACT FOR REAGENT AND RESOURCE SHARING
- EXPERIMENTAL MODEL AND SUBJECT DETAILS
  - Flies
  - Genotypes
- METHOD DETAILS
  - Cell Dissociation and Sorting
  - RNA Amplification and Library Preparation
  - Analysis of RNA-Seq Data
  - Clusters and Sub-Clusters Generation and Analysis
  - DNA Binding Protein Screen
  - Gene Enrichment Analysis
  - Clone Generation
  - Immunohistochemistry
  - Polyclonal Antibodies Generation
  - Construction of CRISPR Mutant Flies
- DATA AND SOFTWARE AVAILABILITY
- QUANTIFICATION AND STATISTICAL ANALYSIS
  - Quantification of Pruning Severity
  - Quantification of Antibody Staining
  - Correlation Analyses

SUPPLEMENTAL INFORMATION

Supplemental Information includes seven figures and seven tables and can be found with this article online at https://doi.org/10.1016/j.devcel.2018.09.013.

ACKNOWLEDGMENTS

We thank J. Casanova, T. Lee, D. Montell, F. Yu, the Kyoto (DGRC), FlyORF, and Bloomington Stock Centers for reagents; A. Tanai for conceptual discussion about data analyses; O. Golani for assistance with image analysis; R. Rotkopf for assistance with statistics; T. Meir-Salame for assistance with the FACS; A. Lubart and M. Zoosman for technical assistance; and A. Yaron, M. Schuldiner, and the members of the Schuldiner lab, especially H. Meltzer and S. Yaniv, for discussions and critical reading of the manuscript. Monoclonal antibodies were obtained from the Developmental Studies Hybridoma Bank developed under the auspices of the NICHD and maintained by the University of Iowa. This work was supported by the European Research Council (ERC) consolidator grant "AxonGrowth." Fly food for this project was funded by the Women Health Research Center.

I. Amit is supported by the Chan Zuckerberg Initiative (CZI); the HHMI International Scholar award; the European Research Council Consolidator Grant (ERC-COG) 724471-HemTree2.0; an MRA Established Investigator Award (509044); the Israel Science Foundation (703/15); the Ernest and Bonnie Beutler Research Program for Excellence in Genomic Medicine; the Helen and Martin Kimmel award for innovative investigation; a Minerva Stiftung research grant; the Israeli Ministry of Science, Technology, and Space; the David and Fela Shapell Family Foundation; the NeuroMac DFG/Transregional Collaborative Research Center Grant; an International Progressive MS Alliance/NMSS PA-1604-08459; and an Adelis Foundation grant.

AUTHOR CONTRIBUTIONS

I. Alyagor designed, performed, and analyzed experiments; performed bioinformatic analyses; and wrote the manuscript. V.B., N.M.-K., and N.I.-Z. designed, performed, and analyzed specific experiments. H.K.-S. performed and analyzed the RNA-seq experiments. E.D. performed bioinformatic analyses. O.M. developed image quantification methods. I. Amit contributed to project design and interpretation of the data and provided comments on the manuscript. O.S. led the project, designed experiments, interpreted results, and wrote the manuscript.

DECLARATION OF INTERESTS

The authors declare no competing interests.

Received: July 18, 2017
Revised: June 26, 2018
Accepted: September 10, 2018
Published: October 8, 2018

REFERENCES

Awasaki, T., Tatsumi, R., Takahashi, K., Arai, K., Nakanishi, Y., Ueda, R., and Ito, K. (2006). Essential role of the apoptotic cell engulfment genes draper and ced-6 in programmed axon pruning during Drosophila metamorphosis. Neuron *50*, 855867.

Bai, J., Uehara, Y., and Montell, D.J. (2000). Regulation of invasive cell behavior by taiman, a Drosophila protein related to AIB1, a steroid receptor coactivator amplified in breast cancer. Cell *103*, 1047–1058.

Barkai, N., and Leibler, S. (2000). Circadian clocks limited by noise. Nature *403*, 267–268.

Biggin, M.D., and Tjian, R. (1989). Transcription factors and the control of Drosophila development. Trends Genet. *5*, 377–383.

Bischof, J., Björklund, M., Furger, E., Schertel, C., Taipale, J., and Basler, K. (2013). A versatile platform for creating a comprehensive UAS-ORFeome library in Drosophila. Development *140*, 2434–2442.

Boulanger, A., Clouet-Redt, C., Farge, M., Flandre, A., Guignard, T., Fernando, C., Juge, F., and Dura, J.M. (2011). ftz-f1 and Hr39 opposing roles on EcR expression during Drosophila mushroom body neuron remodeling. Nat. Neurosci. *14*, 37–44.

Briggs, J.A., Weinreb, C., Wagner, D.E., Megason, S., Peshkin, L., Kirschner, M.W., and Klein, A.M. (2018). The dynamics of gene expression in vertebrate embryogenesis at single-cell resolution. Science *360*, https://doi.org/10.1126/science.aar5780.

Brill, M.S., Kleele, T., Ruschkies, L., Wang, M., Marahori, N.A., Reuter, M.S., Hausrat, T.J., Weigand, E., Fisher, M., Ahles, A., et al. (2016). Branch-specific microtubule destabilization mediates axon branch loss during neuromuscular synapse elimination. Neuron *92*, 845–856.

Cherbas, L., Hu, X., Zhimulev, I., Belyaeva, E., and Cherbas, P. (2003). EcR isoforms in Drosophila: testing tissue-specific requirements by targeted blockade and rescue. Development *130*, 271–284.

Cocchi, E., Drago, A., and Serretti, A. (2016). Hippocampal pruning as a new theory of schizophrenia etiopathogenesis. Mol. Neurobiol. *53*, 2065–2081.

Cosker, K.E., Pazyra-Murphy, M.F., Fenstermacher, S.J., and Segal, R.A. (2013). Target-derived neurotrophins coordinate transcription and transport of bclw to prevent axonal degeneration. J. Neurosci. *33*, 5195–5207.

Dixit, A., Parnas, O., Li, B., Chen, J., Fulco, C.P., Jerby-Arnon, L., Marjanovic, N.D., Dionne, D., Burks, T., Raychowdhury, R., et al. (2016). Perturb-seq: dissecting molecular circuits with scalable single-cell RNA profiling of pooled genetic screens. Cell *167*, 1853–1866.e17.

Edgar, R., Domrachev, M., and Lash, A.E. (2002). Gene Expression Omnibus: NCBI gene expression and hybridization array data repository. Nucleic Acids Res. *30*, 207–210.

Erijman, A., Dantes, A., Bernheim, R., Shifman, J.M., and Peleg, Y. (2011). Transfer-PCR (TPCR): a highway for DNA cloning and protein engineering. J. Struct. Biol. *175*, 171–177.

Farrell, J.A., Wang, Y., Riesenfeld, S.J., Shekhar, K., Regev, A., and Schier, A.F. (2018). Single-cell reconstruction of developmental trajectories during zebrafish embryogenesis. Science *360*, https://doi.org/10.1126/science.aar3131.

Hakim, Y., Yaniv, S.P., and Schuldiner, O. (2014). Astrocytes play a key role in Drosophila mushroom body axon pruning. PLoS One *9*, e86178.

Heinz, S., Benner, C., Spann, N., Bertolino, E., Lin, Y.C., Laslo, P., Cheng, J.X., Murre, C., Singh, H., and Glass, C.K. (2010). Simple combinations of lineage-determining transcription factors prime cis-regulatory elements required for macrophage and B cell identities. Mol. Cell *38*, 576–589.

Hoopfer, E.D., Penton, A., Watts, R.J., and Luo, L. (2008). Genomic analysis of Drosophila neuronal remodeling: a role for the RNA-binding protein Boule as a negative regulator of axon pruning. J. Neurosci. *28*, 6092–6103.

Issman-Zecharya, N., and Schuldiner, O. (2014). The PI3K class III complex promotes axon pruning by downregulating a Ptc-derived signal via endosome-lysosomal degradation. Dev. Cell *31*, 461–473.

Jaitin, D.A., Kenigsberg, E., Keren-Shaul, H., Elefant, N., Paul, F., Zaretsky, I., Mildner, A., Cohen, N., Jung, S., Tanay, A., et al. (2014). Massively parallel single-cell RNA-seq for marker-free decomposition of tissues into cell types. Science *343*, 776–779.

Jaitin, D.A., Weiner, A., Yofe, I., Lara-Astiaso, D., Keren-Shaul, H., David, E., Salame, T.M., Tanay, A., van Oudenaarden, A., and Amit, I. (2016). Dissecting immune circuits by linking CRISPR-pooled screens with single-cell RNA-seq. Cell *167*, 1883–1896.e15.

Jang, A.C., Chang, Y.C., Bai, J., and Montell, D. (2009). Border-cell migration requires integration of spatial and temporal signals by the BTB protein Abrupt. Nat. Cell Biol. *11*, 569–579.

Kim, D., Langmead, B., and Salzberg, S.L. (2015). HISAT: a fast spliced aligner with low memory requirements. Nat. Methods *12*, 357–360.

King-Jones, K., and Thummel, C.S. (2005). Nuclear receptors–a perspective from Drosophila. Nat. Rev. Genet. *6*, 311–323.

Kirilly, D., Gu, Y., Huang, Y., Wu, Z., Bashirullah, A., Low, B.C., Kolodkin, A.L., Wang, H., and Yu, F. (2009). A genetic pathway composed of Sox14 and Mical governs severing of dendrites during pruning. Nat. Neurosci. *12*, 1497–1505.

Klingler, M., and Gergen, J.P. (1993). Regulation of runt transcription by Drosophila segmentation genes. Mech. Dev. *43*, 3–19.

Kozhemyakina, E., Lassar, A.B., and Zelzer, E. (2015). A pathway to bone: signaling molecules and transcription factors involved in chondrocyte development and maturation. Development *142*, 817–831.

Kuo, C.T., Jan, L.Y., and Jan, Y.N. (2005). Dendrite-specific remodeling of Drosophila sensory neurons requires matrix metalloproteases, ubiquitin-proteasome, and ecdysone signaling. Proc. Natl. Acad. Sci. USA *102*, 15230–15235.

Kuo, C.T., Zhu, S., Younger, S., Jan, L.Y., and Jan, Y.N. (2006). Identification of E2/E3 ubiquitinating enzymes and caspase activity regulating Drosophila sensory neuron dendrite pruning. Neuron *51*, 283–290.

Lee, T., and Luo, L. (1999). Mosaic analysis with a repressible cell marker for studies of gene function in neuronal morphogenesis. Neuron *22*, 451–461.

Lee, T., Marticke, S., Sung, C., Robinow, S., and Luo, L. (2000). Cell-autonomous requirement of the USP/EcR-B ecdysone receptor for mushroom body neuronal remodeling in Drosophila. Neuron *28*, 807–818.

Lin, S., Huang, Y., and Lee, T. (2009). Nuclear receptor unfulfilled regulates axonal guidance and cell identity of Drosophila mushroom body neurons. PLoS One *4*, e8392.

Liu, Z., Yang, C.P., Sugino, K., Fu, C.C., Liu, L.Y., Yao, X., Lee, L.P., and Lee, T. (2015). Opposing intrinsic temporal gradients guide neural stem cell production of varied neuronal fates. Science *350*, 317–320.

Loncle, N., Agromayor, M., Martin-Serrano, J., and Williams, D.W. (2015). An ESCRT module is required for neuron pruning. Sci. Rep. *5*, 8461.

Loncle, N., and Williams, D.W. (2012). An interaction screen identifies headcase as a regulator of large-scale pruning. J. Neurosci. *32*, 17086–17096.

Love, M.I., Huber, W., and Anders, S. (2014). Moderated estimation of fold change and dispersion for RNA-seq data with DESeq2. Genome. Biol. *15*, 550.

Luo, L., and O'Leary, D.D. (2005). Axon retraction and degeneration in development and disease. Annu. Rev. Neurosci. *28*, 127–156.

Marin, E.C., Watts, R.J., Tanaka, N.K., Ito, K., and Luo, L. (2005). Developmentally programmed remodeling of the Drosophila olfactory circuit. Development *132*, 725–737.

Matcovitch-Natan, O., Winter, D.R., Giladi, A., Vargas Aguilar, S., Spinrad, A., Sarrazin, S., Ben-Yehuda, H., David, E., Zelada González, F., Perrin, P., et al. (2016). Microglia development follows a stepwise program to regulate brain homeostasis. Science *353*, aad8670.

Molyneaux, B.J., Goff, L.A., Brettler, A.C., Chen, H.H., Hrvatin, S., Rinn, J.L., and Arlotta, P. (2015). DeCoN: genome-wide analysis of in vivo transcriptional dynamics during pyramidal neuron fate selection in neocortex. Neuron *85*, 275–288.

Öztürk-Çolak, A., Moussian, B., Araújo, S.J., and Casanova, J. (2016). A feedback mechanism converts individual cell features into a supracellular ECM structure in Drosophila trachea. Elife *5*, https://doi.org/10.7554/eLife.09373.

Port, F., and Bullock, S.L. (2016). Augmenting CRISPR applications in Drosophila with tRNA-flanked sgRNAs. Nat. Methods *13*, 852–854.

Port, F., Chen, H.M., Lee, T., and Bullock, S.L. (2014). Optimized CRISPR/Cas tools for efficient germline and somatic genome engineering in Drosophila. Proc. Natl. Acad. Sci. USA *111*, E2967–E2976.

Potthoff, M.J., and Olson, E.N. (2007). MEF2: a central regulator of diverse developmental programs. Development *134*, 4131–4140.

Rabinovich, D., Yaniv, S.P., Alyagor, I., and Schuldiner, O. (2016). Nitric oxide as a switching mechanism between axon degeneration and regrowth during developmental remodeling. Cell *164*, 170–182.

Ren, Q., Yang, C.P., Liu, Z., Sugino, K., Mok, K., He, Y., Ito, M., Nern, A., Otsuna, H., and Lee, T. (2017). Stem cell-intrinsic, seven-up-triggered temporal factor gradients diversify intermediate neural progenitors. Curr. Biol. *27*, 1303–1313.

Schoenmann, Z., Assa-Kunik, E., Tiomny, S., Minis, A., Haklai-Topper, L., Arama, E., and Yaron, A. (2010). Axonal degeneration is regulated by the apoptotic machinery or a NAD^+-sensitive pathway in insects and mammals. J. Neurosci. *30*, 6375–6386.

Schubiger, M., Wade, A.A., Carney, G.E., Truman, J.W., and Bender, M. (1998). Drosophila EcR-B ecdysone receptor isoforms are required for larval molting and for neuron remodeling during metamorphosis. Development *125*, 2053–2062.

Schuldiner, O., and Yaron, A. (2015). Mechanisms of developmental neurite pruning. Cell Mol. Life Sci. *72*, 101–119.

Sekar, A., Bialas, A.R., de Rivera, H., Davis, A., Hammond, T.R., Kamitaki, N., Tooley, K., Presumey, J., Baum, M., Van Doren, V., et al. (2016). Schizophrenia risk from complex variation of complement component 4. Nature *530*, 177–183.

Shigeoka, T., Jung, H., Jung, J., Turner-Bridger, B., Ohk, J., Lin, J.Q., Amieux, P.S., and Holt, C.E. (2016). Dynamic axonal translation in developing and mature visual circuits. Cell *166*, 181–192.

Simon, D.J., Weimer, R.M., McLaughlin, T., Kallop, D., Stanger, K., Yang, J., O'Leary, D.D.M., Hannoush, R.N., and Tessier-Lavigne, M. (2012). A caspase cascade regulating developmental axon degeneration. J. Neurosci. *32*, 17540–17553.

Tasdemir-Yilmaz, O.E., and Freeman, M.R. (2014). Astrocytes engage unique molecular programs to engulf pruned neuronal debris from distinct subsets of neurons. Genes Dev. *28*, 20–33.

Thomas, M.S., Davis, R., Karmiloff-Smith, A., Knowland, V.C., and Charman, T. (2016). The over-pruning hypothesis of autism. Dev. Sci. *19*, 284–305.

Truman, J.W. (1990). Metamorphosis of the central nervous system of Drosophila. J. Neurobiol. *21*, 1072–1084.

Truman, J.W., Talbot, W.S., Fahrbach, S.E., and Hogness, D.S. (1994). Ecdysone receptor expression in the CNS correlates with stage-specific responses to ecdysteroids during Drosophila and Manduca development. Development *120*, 219–234.

Unger, T., Jacobovitch, Y., Dantes, A., Bernheim, R., and Peleg, Y. (2010). Applications of the Restriction Free (RF) cloning procedure for molecular manipulations and protein expression. J. Struct. Biol. *172*, 34–44.

Wagner, D.E., Weinreb, C., Collins, Z.M., Briggs, J.A., Megason, S.G., and Klein, A.M. (2018). Single-cell mapping of gene expression landscapes and lineage in the zebrafish embryo. Science *360*, 981–987.

Watts, R.J., Hoopfer, E.D., and Luo, L. (2003). Axon pruning during Drosophila metamorphosis: evidence for local degeneration and requirement of the ubiquitin-proteasome system. Neuron *38*, 871–885.

Williams, D.W., Kondo, S., Krzyzanowska, A., Hiromi, Y., and Truman, J.W. (2006). Local caspase activity directs engulfment of dendrites during pruning. Nat. Neurosci. *9*, 1234–1236.

Williams, D.W., and Truman, J.W. (2005). Cellular mechanisms of dendrite pruning in Drosophila: insights from in vivo time-lapse of remodeling dendritic arborizing sensory neurons. Development *132*, 3631–3642.

Yaniv, S.P., Issman-Zecharya, N., Oren-Suissa, M., Podbilewicz, B., and Schuldiner, O. (2012). Axon regrowth during development and regeneration following injury share molecular mechanisms. Curr. Biol. *22*, 1774–1782.

Yaniv, S.P., and Schuldiner, O. (2016). A fly's view of neuronal remodeling. Wiley Interdiscip. Rev. Dev. Biol. *5*, 618–635.

Yu, F., and Schuldiner, O. (2014). Axon and dendrite pruning in Drosophila. Curr. Opin. Neurobiol. *27*, 192–198.

Zhang, H., Wang, Y., Wong, J.J., Lim, K.L., Liou, Y.C., Wang, H., and Yu, F. (2014). Endocytic pathways downregulate the L1-type cell adhesion molecule neuroglian to promote dendrite pruning in Drosophila. Dev. Cell *30*, 463–478.

STAR★METHODS

KEY RESOURCES TABLE

REAGENT or RESOURCE	SOURCE	IDENTIFIER
Antibodies		
Chicken anti GFP 1:500	AVES	Cat# GFP-1020; RRID: AB_10000240
Mouse monoclonal anti FasII 1:25	Developmental Studies Hybridoma Bank (DSHB)	Cat# 1D4; RRID: AB_528235
Rabbit anti Mamo 1:5000	This study	Cat# Mamo; RRID: AB_2665566
Mouse anti Sox14 1:200	Kirilly et al. (2009)	Cat# Sox14; RRID: AB_2568322
Mouse monoclonal anti EcR-B1 1:25	DSHB	Cat# AD4.4; RRID: AB_2154902
Rabbit anti Tai 1:500	Bai et al. (2000)	
Goat anti chicken FITC 1:300	Invitrogen	Cat# A16055; RRID: AB_2534728
Goat anti mouse Alexa fluor 647 1:300	Invitrogen	Cat# A32728; RRID: AB_2633277
Goat anti rabbit Alexa fluor 647 1:300	Invitrogen	Cat# A32733; RRID: AB_2633282
Bacterial and Virus Strains		
DH5α	N/A	N/A
Chemicals, Peptides, and Recombinant Proteins		
Cell Dissociation Solution	Sigma Aldrich	Cat# C1544
Collagenase/dispase mix	Roche	Cat# 10269638001
Peptides used for anti-Mamo antibody generation: REPEREPDRLRP HQRQVMDDRLEQDVDE	This study	N/A
Critical Commercial Assays		
Pico pure RNA isolation kit	Life Technologies	Cat# KIT0204
Gibson assembly	NEB	Cat# E5510S
Deposited Data		
Raw data files for Developmental seq and Perturbation seq	NCBI Gene Expression Omnibus	GEO: GSE101946
Experimental Models: Organisms/Strains		
w^{1118}; UAS-RedStinger/CyO	BDSC	BDSC: 8546
w^{1118}; GMR71G10-GAL4 (in attP2)	BDSC	BDSC: 39604
y,w; GMR71G10-GAL4 (in attP40)	This study	N/A
w*; NP3061-GAL4	DGRC	DGRC: 104360
C155-GAL4	BDSC	BDSC: 458
w^{1118};201Y-GAL4	BDSC	BDSC: 4440
w*; alrm-GAL4/ CyO; Dr1/TM3, Sb1	BDSC	BDSC: 67031
y^{1}, w^{67c23}; mb247-GAL80	BDSC	BDSC: 64306
y,w,TubP-Gal80, hsflp,19A; UAS-CD8:GFP,201Y-Gal4/CyO;	This study based on BDSC lines	N/A
hsflp122, 10xUAS-IVS-CD8:GFP; TubP-Gal80,40A/Cyo; GMR71G10-Gal4/Tm6,Tb	This study based on BDSC lines	N/A
hsflp122, 10xUAS-IVS-CD8:GFP;Tub-Gal80,G13/Cyo; GMR71G10-Gal4/Tm6,Tb	This study based on BDSC lines	N/A
y,w, hsflp122, 10xUAS-IVS-CD8:GFP;GMR71G10-Gal4/Cyo; TubP-Gal80,2A/TM6,Tb	This study based on BDSC lines	N/A
hsflp122,10xUAS-IVS-CD8:GFP;201Y-Gal4,UAS-CD8:GFP/ CyO; TubP-Gal80,2A,82B, TubP-Gal80/TM6,Tb	This study based on BDSC lines	N/A

(*Continued on next page*)

Continued

REAGENT or RESOURCE	SOURCE	IDENTIFIER
w*; 10XUAS-IVS-mCD8::GFP (in attP2)	BDSC	BDSC: 32185
w*; 10XUAS-IVS-mCD8::GFP (in attP40)	BDSC	BDSC: 32186
usp^{3}, w*, 19A/FM7c	BDSC	BDSC: 64295
y,w; 40A,G13, $Sox14^{CRISPR\Delta1}$/Cyo	This study	N/A
y,w; 40A,G13, $chinmo^{CRISPR\Delta1}$/Cyo	This study	N/A
y,w,$mamo^{indel1}$,19A/FM7	This study	N/A
E75Δ51,2A/Cyo	Based on BDSC line	BDSC: 23652
dpy^{ov1},tai[61G1],40A/CyO	BDSC	BDSC: 6379
y,w; 40A,G13, $Sox14^{\Delta15}$/Cyo	Gift from Kirilly et al. (2009)	N/A
y^{1},sc*,v^{1}; UAS-mamo $RNAi^{TRiP.HMS02823}$ (in attP40)	BDSC	BDSC: 44103
y^{1},v^{1};UAS- $RNAi^{TRiP.HMJ22371}$ (in attp40)	BDSC	BDSC: 58286
y^{1},sc*,v^{1}; UAS-tai $RNAi^{TRiP.HMS00673}$ (in attP2)	BDSC	BDSC: 32885
y,w;UAS-$E75^{miRNA}$ (in attp16)/CyO	Gift from Lin et al. (2009)	N/A
y^{1},sc*,v^{1}; UAS-Sox14 $RNAi^{TRiP.HMS00103}$ (in attP2)	BDSC	BDSC: 34794
y^{1},sc*,v^{1}; UAS-chinmo $RNAi^{TRiP.HMS00036}$ (in attP2)/TM3	BDSC	BDSC: 33638
y^{1},sc*,v^{1}; UAS-unf $RNAi^{TRiP.HMS01951}$ (in attP2)	BDSC	BDSC: 39032
UAS-Blimp-1	Gift from Öztürk-Çolak et al. (2016)	N/A
UAS-HmgZ-3xHA (in attp86Fb)	FlyORF	FlyORF: F001885
UAS-pros.L,w*	BSDC	BDSC: 32244
UAS-Hr3-3xHA (in attp86Fb)	FlyORF	FlyORF: F000034
W^{1118}; UAS-$EcR.B1^{DN(\Delta C655.W650A)}$	BDSC	BDSC: 6872
w*; sna^{Sco}/CyO; UAS-$tai^{\Delta BHLH}$	BDSC	BDSC: 28273
w*; sna^{Sco}/CyO; UAS- $tai^{nls.LXXLL-GFP}$	BDSC	BDSC: 28272
Lines for the screen were obtained from the TRiP collection (BDSC) and FlyORF. For genes without available TRiP collection line in BDSC, alternative RNAi lines were obtained from the GD and KK RNAi collection (VDRC). This Key Resource Table includes only those lines for which images were included in the manuscript.	N/A	N/A
Oligonucleotides		
gRNAs specific sequence for Sox14 deletion: GATGGCGTCCGCCTCCACGA ACACAGTGGACACCAGAACT	This study	N/A
gRNAs specific sequence for chinmo deletion: GTAGCATCACTGCTGGCACCA GCTTGGTCGTAGGTGGTCTC	This study	N/A
gRNAs specific sequence for mamo deletion: GCAGTGAGCACTACTGCTTG CTCGGCTTGTTCCTCGTACT	This study	N/A
Primers for Sox14 deletion check: F' AAGCCACAGAGAATCGGAGC R' TTATCGTGTGCGGCGTAGTT	This study	N/A
Primers for chinmo deletion check: F' TTCTCGTTGCAGCATTTGGC R' GCCTGCAAAAAGTTGGTGGT	This study	N/A
Primers for mamo deletion check: F' TTCCATACGCTCGCTCTTCG R' AGACTTACCGACTCGTGGGA	This study	N/A
Recombinant DNA		
pCFD4	Port et al. (2014)	N/A
pCFD5	Port and Bullock (2016)	N/A

(*Continued on next page*)

Continued

REAGENT or RESOURCE	SOURCE	IDENTIFIER
Software and Algorithms		
MATLAB R2016a software	MathWorks	N/A
HISAT v.0.1.5	Kim et al. (2015)	https://github.com/infphilo/hisat
DEseq2	Love et al. (2014)	N.A
Gene-e v.3.0.215	Broad Institute, Inc.	https://software.broadinstitute.org/GENE-E/
HOMER software	Heinz et al. (2010)	N/A
FIJI	Image J	https://imagej.net/Fiji/Downloads
FlowJo v10	FlowJo, LLC	N/A
Other		
Illumina NextSeq 500 sequencer	Illumina	N/A
BD FACSAria Fusion flow cytometer	BD Bioscience	N/A
Zeiss LSM 710 and 800 confocal microscope	Zeiss	N/A
40x 1.3 NA oil immersion lens	Zeiss	N/A

CONTACT FOR REAGENT AND RESOURCE SHARING

Further information and requests for resources and reagents should be directed to and will be fulfilled by the Lead Contact, Oren Schuldiner (oren.schuldiner@weizmann.ac.il).

EXPERIMENTAL MODEL AND SUBJECT DETAILS

Flies

All fly strains were reared under standard laboratory conditions at 25°C on molasses containing food. Males and females were chosen at random. Developmental stage is referred to in the relevant places while adult refers to 3-5 days post eclosion.

For a detailed list of the stocks and their source, see Key Resource Table.

Sox14$^{\Delta 15}$ was generated and kindly provided by Dr. Fengwei Yu (Kirilly et al., 2009). UAS-Blimp-1 was generated and kindly provided by Dr. Jordi Casanova (Öztürk-Çolak et al., 2016). UAS-E75^{miRNA} was generated and kindly provided by Dr. Tzumin Lee (Lin et al., 2009). UAS-HmgZ.ORF.3xHA, UAS-Hr3.ORF.3xHA, UAS-Mef2.ORF.3xHA, UAS-ab.ORF.3xHA and UAS-Pep.ORF.3xHA was were obtained from FlyORF (University of Zurich in Switzerland; Bischof et al., 2013). RNAi lines were obtained from the Vienna Drosophila RNAi Center (VDRC) or from Bloomington Drosophila Stock Center (BDSC), USA. NP3061-GAL4 obtained from Kyoto Drosophila Genetic Resource Center (DGRC). All other lines were also obtained from the BDSC.

R71G10 on chromosome 2 was generated by amplifying the sequences, as determined in the FlyLight database, cloned into pBPGUw using the Gateway system and injected into attP40 landing site using ΦC31 intergation (BestGene).

Genotypes

hsFLP is y,w,hsFLP122; GFP is GFP; 19A, G13, 40A, 2A and 82B are FRTs on X, 2R, 2L, 3L and 3R respectively; 71G10 is R71G10-GAL4; 201Y is 201y-GAL4; G80 is TubsP-Gal80. Males and females were used interchangeably but only the female genotype is mentioned.

Figure 1 and 2

y,w/+; UAS-RedStinger/+;71G10/+
y,w/w; UAS-RedStinger/+;NP3061-GAL4/+
y,w/C155-GAL4; UAS-RedStinger/MB247-GAL80
UAS-RedStinger/ CyO; alrm-Gal4, GFP, UAS-Dcr2/TM6,tb

Figure 3

(D) hsFLP, GFP / y,w; G80,40A/40A; 71G10/+
(E) y,w,G80,hsFLP,19A/ y,w,*mamo* $^{CRISPR\Delta 1}$,19A; GFP,201Y/+
(F) hsFLP,GFP/ y,w; G80,G13/ 40A, G13, *Sox14*$^{CRISPR\Delta 1}$; 71G10/+
(G) hsFLP,GFP/ y,w; 71G10/+; G80,2A/ *E75*$^{\Delta 51}$, 2A
(H) hsFLP,GFP /+; G80, 40A/*tal*^{61G1}, 40A; 71G10/+
(I) hsFLP,GFP / y,w; G80,40A/ *chinmo*$^{CRISPR\Delta 1}$, 40A, G13; 71G10/+
(J) y,w;GFP /+;71G10/+
(K) y,w/+;GFP /UAS-Blimp-1; 71G10/+;
(L) y,w/+;GFP /+; 71G10/ UAS-HmgZ.ORF.3xHA;

(M) y,w/UAS-pros.L, w; GFP /+;71G10/+;
(O) hsFLP, GFP /+; G80, 40A/*tai*^{61G1}, 40A; 71G10/UAS-tai$^{\Delta BHLH}$
(P) y,w; GFP /+; 71G10/UAS-tai$^{nls.LXXLL-GFP}$

Figure 4

(A) Control: y,w; GFP /+;71G10/+.
y,w; UAS-RedStinger/+;71G10/+.
EcR^{DN}: y,w; GFP / UAS-EcR$^{DN(\Delta C655.W650A)}$; 71G10/+
y,w; UAS-RedStinger/ UAS-EcR$^{DN(\Delta C655.W650A)}$; 71G10/+
Sox14-RNAi: y,w/y,sc,v; GFP /+;71G10/UAS-Sox14 RNAi$^{TRiP.HMS00103}$
y,w/y,sc,v; UAS-RedStinger /+; 71G10/UAS-Sox14-RNAi$^{TRiP.HMS00103}$
E75-RNAi: y,w/y,w; GFP / UAS-E75-RNAi^{miRNA}; 71G10/+
y,w/y,w; UAS-RedStinger / UAS-E75-RNAi^{miRNA}; 71G10/+

Figure 5

(B,D) hsFLP / y,w; 201Y,GFP/ UAS-E75-RNAi^{miRNA}; G80,2A/ 2A, 82B
(E) hsFLP, GFP /+; G80,40A/*tai*^{61G1}, 40A; 71G10/+
(F) hsFLP, G80, 19A/ *usp*^{3}, w*, 19A; GFP, 201Y /+;

Figure S1

y,w; GFP /+; 71G10 /+
Figure S2
(A,B) y,w/+; UAS-RedStinger/ GFP ; 71G10 /+
(C,D) y,w/+; UAS-RedStinger/+;71G10/+

Figure S4

(A) Lines for the screen were obtained from the TRiP collection (BDSC) and FlyORF and other sources as indicated in Table S7. For genes without available TRiP collection line in BDSC, alternative RNAi lines were obtained from the GD and KK RNAi collection (VDRC). The Key Resource Table includes those lines for which images were included in the manuscript.
(B_1-B_3) y,w; GFP /+; 71G10 /+
(C_1-C_3) y,w/+; GFP /UAS-EcR-RNAi$^{TRiP.HMJ22371}$; 71G10 /+
(D_1) y,w/y,sc,v; GFP /+; 71G10 /UAS-tai-RNAi$^{TRiP.HMS00673}$
(D_2-D_3) hsFLP, GFP /+; G80,40A/*tai*^{61G1}, 40A; 71G10/+
(E_1) y,w/y,sc,v; GFP /+; 71G10 /UAS-Sox14-RNAi$^{TRiP.HMS00103}$
(E_2-E_3) hsFLP,GFP/ y,w; G80,G13/ 40A, G13, *Sox14*$^{CRISPR\Delta1}$; 71G10/+
(F_1) y,w/y,sc,v; GFP / UAS-mamo-RNAi$^{TRiP.HMS02823}$; 71G10 /+
(F_2-F_3) y,w,G80,hsFLP,19A/ y,w,*mamo*$^{CRISPR\Delta1}$,19A; GFP,201Y/+
(G_1) y,w/y,sc,v; GFP /+; 71G10 /UAS-chinmo-RNAi$^{TRiP.HMS00036}$ (reared on 29°C)
(G_2-G_3) hsFLP,GFP / y,w; G80,40A/ *chinmo*$^{CRISPR\Delta1}$, 40A, G13; 71G10/+
(H_1-H_3) y,w; 201Y, GFP /UAS-E75-RNAi^{miRNA}
(I_1-I_2) y,w/y,sc,v; GFP /+; 71G10 /UAS-unf-RNAi$^{TRiP.HMS01951}$
(J_1-J_2) y,w/UAS-pros.L, w; GFP /+;71G10/+;
(K_1-K_2) y,w/+; GFP /UAS-Blimp-1; 71G10/+;
(L_1-L_2) y,w/+; GFP /+;71G10/ UAS-HmgZ.ORF.3xHA;

Figure S5

(A-D) y,w; GFP;71G10;

Figure S6

(C-D) hsFLP, GFP /+; G80,40A/*tai*^{61G1}, 40A; 71G10/+

Figure S7

(I,M) hsFLP,GFP; 71G10/ UAS-EcR$^{DN(\Delta C655.W650A)}$; G80,2A/ 2A
(J,L) y,w, hsFLP / y,w; 201Y, GFP /UAS-E75-RNAi^{miRNA}; G80,2A/ 2A, 82B
(K,N) hsFLP,GFP/ y,w; G80,G13/ 40A, G13, *Sox14*$^{CRISPR\Delta1}$; 71G10/+
(O) y,w/+; GFP /+;71G10/ UAS-Hr3.ORF.3xHA;
(P) hsFLP,GFP / y,w; G80,40A/ *chinmo*$^{CRISPR\Delta1}$, 40A, G13; 71G10/+

METHOD DETAILS

Cell Dissociation and Sorting

Brains were dissected in a cold Ringer's solution, incubated with collagenase/dispase mix at 29°C (Roche, 15 minutes for larval and pupal brains and 30 minutes for adult brains), washed in dissociation solution (Sigma-Aldrich), mechanically dissociated into single cells and transferred via 35um mesh (Falcon) to eliminate clusters and debris. 1000 DsRed^{+} positive cells were sorted using a 100μm nozzle and low pressure in BD FACSAria Fusion (BD Bioscience) cell sorted directly into 100μl Pico-Pure RNA isolation kit extraction buffer (Life Technologies) followed by RNA extraction using the kit or stored in -80 for later use. To minimize the effect of an injury

response, the samples were kept on ice for the entire procedure from dissection up to the RNA extraction except from the dissociation enzyme incubation.

RNA Amplification and Library Preparation

mRNA was captured using 12 ml of Dynabeads oligo(dT) (Life Technologies), which were washed from unbound total RNA according to the protocol. mRNA was eluted from beads at 85°C with 10 ml of 10 mM Tris-Cl (pH 7.5). We used a derivation of MARS-seq as described (Jaitin et al., 2014), to produce expression libraries with a minimum of three replicates per population. In brief, mRNA was barcoded, converted into cDNA and linearly amplified by T7 in vitro transcription. The resulting RNA was fragmented and converted into an Illumina sequencing-ready library through ligation, RT, and PCR. Prior to sequencing, libraries were evaluated by Qubit fluorometer and TapeStation (Agilent).

Analysis of RNA-Seq Data

The samples were sequenced using Illumina NextSeq 500 sequencer, at a sequencing depth of an average of 3.5 and 5 million reads per sample for the developmental-seq and perturbations-seq, respectively. We aligned the RNA-seq reads to *Drosophila melanogaster* reference genome (DM6, UCSC) using Hisat v0.1.5 with "–sensitive -local" parameters (Kim et al., 2015). Gene annotation were taken from FlyBase.org (Dmel R6.01/Fb_2014_04). Duplicate reads were filtered if they aligned to the same base and had identical unique molecular identifiers (UMI). Expression levels were counted using HOMER software (http://homer.salk.edu) (Heinz et al., 2010). 11,443 genes had at least one read (11,046 in γ neuron samples). For general analyses, we considered genes with reads over the noise threshold (20 reads) in at least two sample resulting in 7,816 genes expressed above this threshold. Significant expression in the γ neurons considered for genes with reads over a second noise threshold (50 reads) in at least two γ neuron samples resulting in 5,211 genes above this threshold. For normalization and statistics, we performed DEseq2 algorithm (Love et al., 2014) on our samples on R platform, which took into account batch effects. All p values presented for RNA-seq data are adjusted p values.

Clusters and Sub-Clusters Generation and Analysis

Our developmental clusters contain 2,671 genes with 50 reads or more in at least two γ neuron samples, a >2-fold and significant ($p<0.01$) change between any two coupled developmental stages or between - L3/6h APF, L3/18h APF, L3/Adults, 6h APF/18h APF, 6h APF/Adults. We performed k-means analysis on the mean expression of the replicates in each time point using correlation distance measure (k=10, MATLAB R2016a).

For the perturbation sequencing we compared the expression of control and perturbed samples, for each developmental stage. Only changes that were statistically significant ($p<0.01$) were considered. To describe the effect of the perturbation compared to the mean expression, we first calculated the normalized expression of each sample in the following manner: the expression value (mean of replicates) plus 20 (a minimal value, determined by our thresholding - to reduce low level expression fluctuation) was $\log_2$ calculated. The average $\log_2$ expression (of the specific gene in the entire perturbation dataset) was then subtracted from these values to give rise to a normalized value that describes its fold change ($\log_2$) expression compared to the average across all conditions.

We then performed k-means analysis for each developmental cluster independently using correlation distance measure (k=2-4, MATLAB R2016a). Sub-clusters that contain less than 30 genes were excluded.

Sub-clusters significance was calculated for the normalized expression using non-parametric Mann-Whitney U test (MATLAB R2016a ranksum function) with Bonferroni correction for multiple comparisons. Significance only shown in Figures 6 and 7 and Table S5 in cases where the average fold change >2.

DNA Binding Protein Screen

Using a database of putative DNA binding proteins (DBP) available in FlyTF.org, we found that our dataset of developmental dynamically expressed genes includes 177 DBPs. For neuronal pruning (clusters II-IV) and regrowth (cluster VI), we chose the 20 genes with the highest expression in the γ neurons for each. From Clusters VII-VIII we focused on the 10 genes with the highest expression and chose only those with significant decrease ($p<0.01$) in expression between third instar larva (L3) and 0h or 6h APF (6 genes).

Gene Enrichment Analysis

Gene enrichment analysis was done using FlyMine (http://www.flymine.org/) and Gene Ontology Consortium (http://www.geneontology.org/).

Clone Generation

Mushroom body MARCM clones were generated as described previously (Lee et al., 2000). Briefly, vials with newly hatched larva were heat shocked 24h after egg laying for 1 hour in 37 degrees Celsius and dissected at the relevant developmental time point.

Immunohistochemistry

Brains were dissected in ringer solution, fixed using 4% paraformaldehyde (PFA) for 20 minutes at room temperature (RT) and washed with PB with 0.3% Triton-X (PBT, 3 immediate washes followed by 3 X 20 minute washes). Non-specific staining was blocked using 5% heat inactivated goat serum in PBT and then samples were subjected to primary antibodies (over-night, 4°C) and secondary antibodies (2 hours at RT) with PBT washes (3 quick washed followed by 3 X 20 minute washes). The brains were mounted on

SlowFade (Invitrogen) and imaged using Zeiss LSM710 or LSM800 confocal microscopes. Images were processed with ImageJ 1.51 (NIH).

Polyclonal Antibodies Generation

In order to generate anti-Mamo antibodies, two short peptides (REPEREPDRLRP and HQRQVMDDRLEQDVDE) that share sequence with all annotated *mamo* isoforms were synthesized, fused to GST and injected together to immunize rabbits. Sera were diluted 1:5000 for tissue immunostaining.

Construction of CRISPR Mutant Flies

Two guide RNA were cloned into pCFD4 using Transfer-PCR (TPCR, for generating $chinmo^{CRISPR\Delta 1}$), Gibson assembly (for generating $Sox14^{CRISPR\Delta 1}$, NEB) or into pCFD5 using restriction free cloning (for generating $mamo^{CRISPR\Delta 1}$) as described previously (Port and Bullock, 2016; Port et al., 2014; Erijman et al., 2011; Unger et al., 2010) to induce large deletion of most of the coding sequence. pCFD4 and pCDFD5 plasmids were injected into attP40 (for $Sox14^{CRISPR\Delta 1}$) and attP86Fb (for $chinmo^{CRISPR\Delta 1}$and $mamo^{CRISPR\Delta 1}$) landing sites using φC31 integration (BestGene). Injected flies were crossed with nanos-Cas9 flies (Bloomington stock #54591). After two generations, single males were crossed with balancers and checked for deletion using specific primers.

DATA AND SOFTWARE AVAILABILITY

The data discussed in this publication have been deposited in NCBI's Gene Expression Omnibus (Edgar et al., 2002) and are accessible through GEO series accession number GEO: GSE101946 (https://www.ncbi.nlm.nih.gov/geo/query/acc.cgi?acc=GSE101946).

QUANTIFICATION AND STATISTICAL ANALYSIS

Quantification of Pruning Severity

In order to quantify the pruning index of MB γ neurons, Z-stacks also counterstained against FasII, were analyzed using a custom-built FIJI macro. Briefly, using this macro, the thickest part of the dorsal α lobe was semi-automatically identified based on FasII staining, and the fluorescence of the GFP positive neurons surrounding it (up to ±10μm radius from the α lobe, excluding the α lobe itself and therefore expected to be unpruned γ) was automatically measured and normalized as compared to the average fluorescence measured in the MB branching point. As another quantification approach, the same images were given to an independent lab member who blindly ranked the severity of the pruning defect, analysis one-way ANOVA was performed and followed by a Dunnett's post-hoc test.

Quantification of Antibody Staining

In order to quantify the levels of antibody staining in γ MARCM clones, images were analyzed using a custom-built FIJI macro. Briefly, we first determined 3 regions of interest (ROIs) – (1) background, outside of the MB cell bodies; (2) control, MB cell bodies outside of the marked clone; and (3) clone. The background subtracted values for the control and clone ROIs were determined for each section and then averaged across sections. Fold change was determined by normalizing by dividing by the control values. Significance of the average fold-change between samples was then determined using standard unpaired 2 tailed students t-test.

Correlation Analyses

Correlation between *EcR*, *E75* and *Sox14* mRNA expression and the sub-clusters conducted using non-parametric spearman rank correlation measure (r_s) between normalized expression of the transcription factor and the sub-cluster average normalized expression in the next time point available (L3 vs 0h APF, 0h APF vs 6h APF, 6h APF vs 12h APF).

Developmental Cell, Volume *47*

Supplemental Information

Combining Developmental and Perturbation-Seq Uncovers Transcriptional Modules Orchestrating Neuronal Remodeling

Idan Alyagor, Victoria Berkun, Hadas Keren-Shaul, Neta Marmor-Kollet, Eyal David, Oded Mayseless, Noa Issman-Zecharya, Ido Amit, and Oren Schuldiner

Figure S1

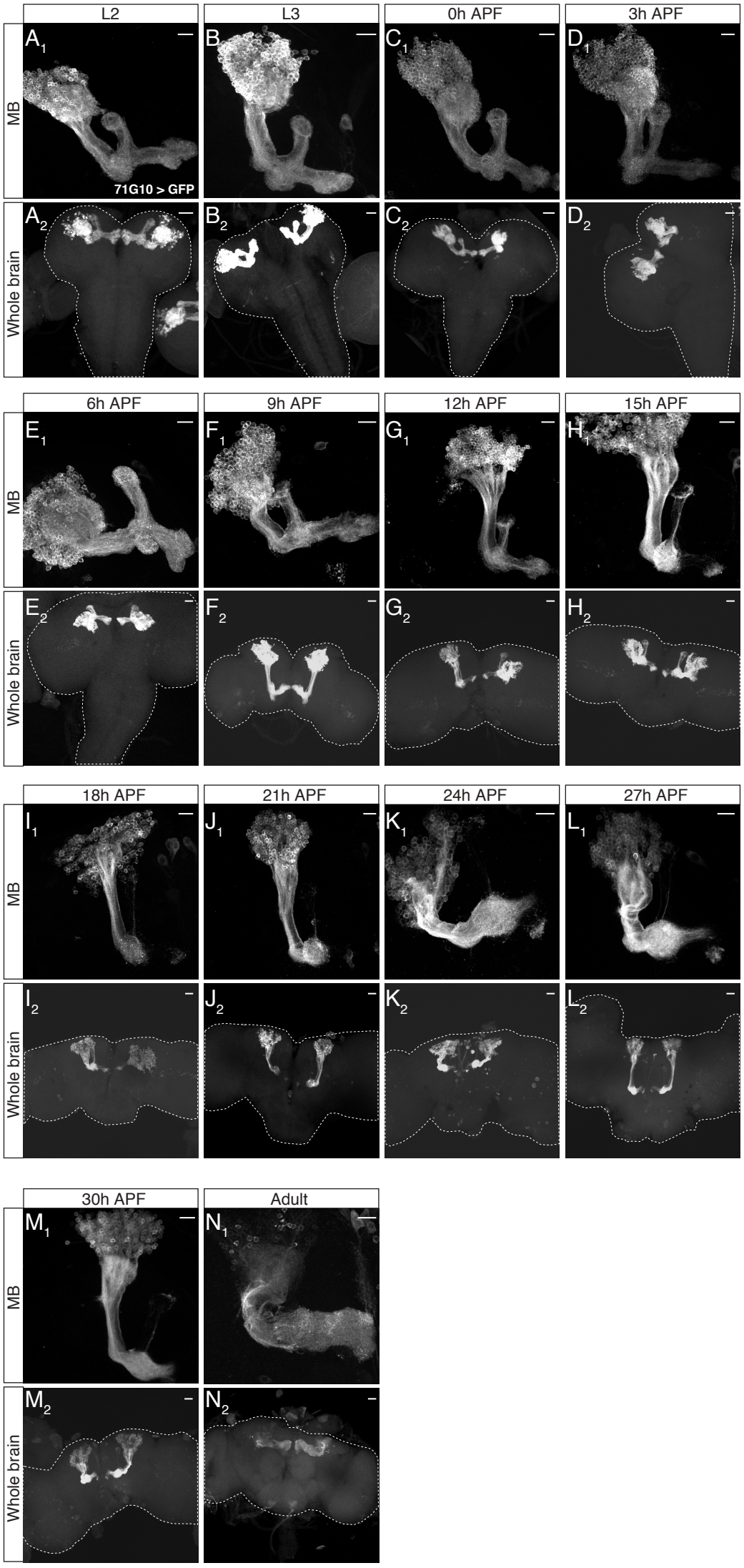
L2
L3
0h APF
3h APF
6h APF
9h APF
12h APF
15h APF
18h APF
21h APF
24h APF
27h APF
30h APF
Adult
MB
Whole brain
71G10 > GFP
A1
A2
B
B2
C1
C2
D1
D2
E1
E2
F1
F2
G1
G2
H1
H2
I1
I2
J1
J2
K1
K2
L1
L2
M1
M2
N1
N2

Figure S1 – **71G10-Gal4 is robustly and almost exclusively expressed in MB γ neurons throughout development, related to Figure 1**

Confocal Z-projections of MB lobe **(A_1-N_1)** and whole brains **(A_2-N_2)** where the γ neurons labeled with mCD8-GFP (GFP) driven by 71G10-Gal4 (71G10), at all the time points taken for the developmental RNA-seq. Whole brain projections are intentionally over exposed in order to emphasize the near absence of labeled neurons outside the MB expressing GFP. Scale bars represent 15 μm for MB-lobes and 30 μm for whole brains.

Figure S2

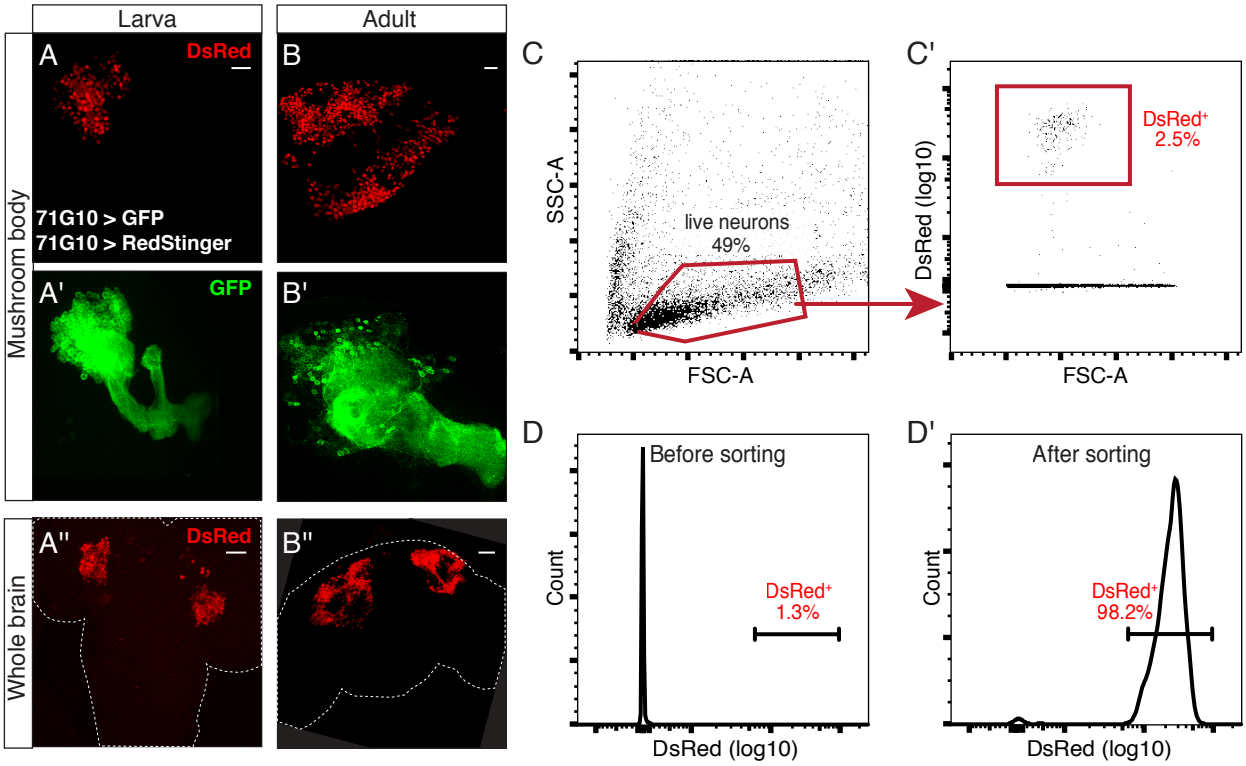
Larva
Adult
Mushroom body
Whole brain
A
DsRed
71G10 > GFP
71G10 > RedStinger
B
A'
GFP
B'
A''
DsRed
B''
C
SSC-A
live neurons
49%
FSC-A
C'
DsRed⁺
2.5%
DsRed (log10)
FSC-A
D
Before sorting
Count
DsRed⁺
1.3%
DsRed (log10)
D'
After sorting
Count
DsRed⁺
98.2%
DsRed (log10)

Figure S2 – **Quality control analyses of cell isolation, related to Figure 1.**

(A) Confocal Z-projections of larval **(A**-**A')** and adult **(B**-**B')** MB γ neurons labeled with nuclear DsRed (RedStinger) and mCD8-GFP (GFP) driven by 71G10-Gal4 (71G10). Low magnification projections that show whole brains (**A''**-**B''**) demonstrate the specificity of 71G10 within the entire brain. Scale bars represent 15 µm for lobes and 30 µm for whole brains.

(C) FACS gating strategy for isolating DsRed positive MB γ neurons from dissociated brains. Forward scatter – FSC is plotted against Side scatter – SSC (**C**) or DsRed expression (**C'**).

(D) FACS analysis of DsRed positive cells from dissociated brains before (**D**) and after (**D'**) positive sorting according to the gating strategy presented in **(C)**. Note that **D** represents the entire cell population resulting in lower $DsRed^+$ cell proportion (1.3%) compared to **C'**, where the analysis includes only live cells that passed a certain SSC and FSC threshold (2.5% $DsRed^+$ cells).

Figure S3

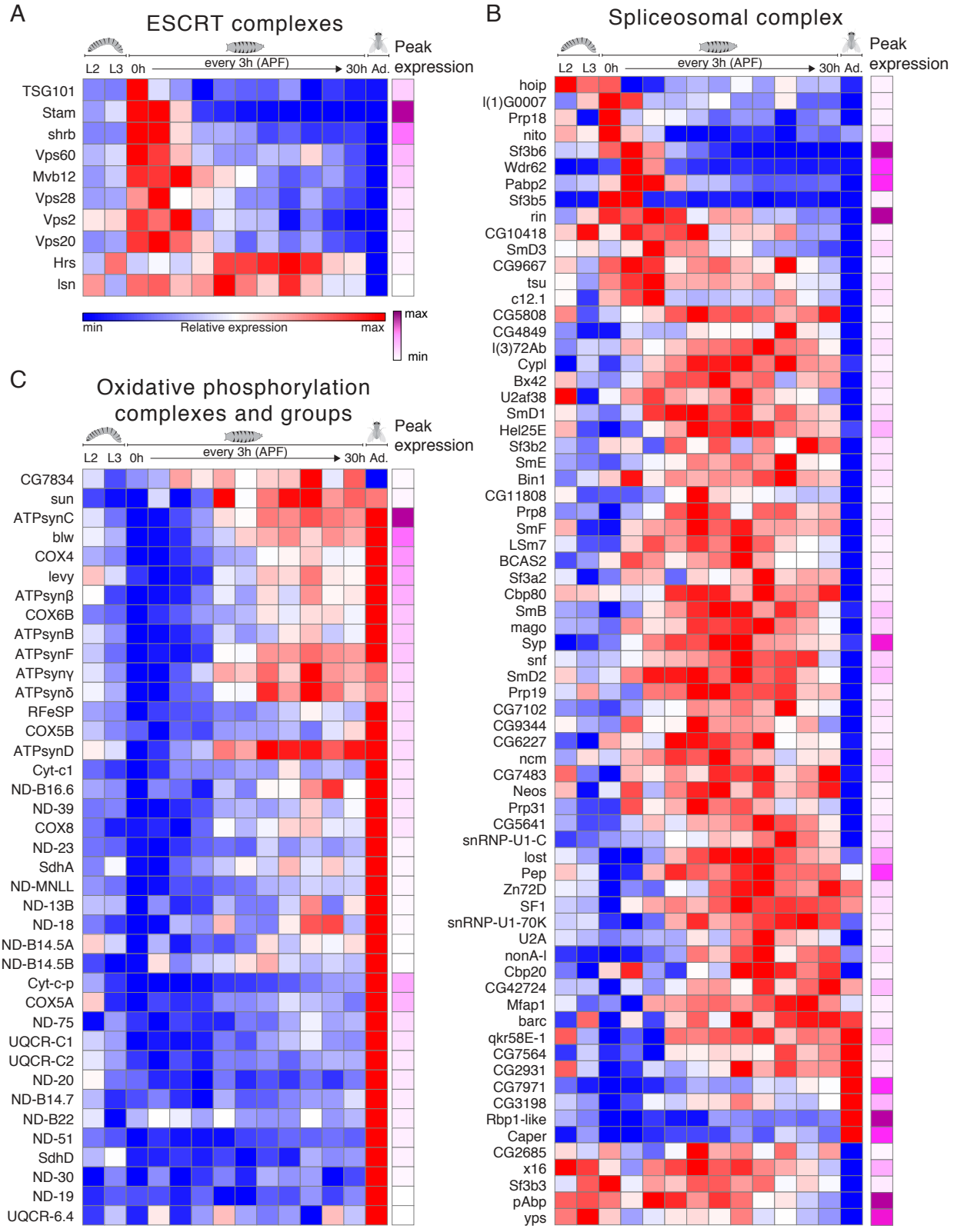
A
ESCRT complexes
L2 L3 0h
every 3h (APF)
30h Ad.
Peak expression
TSG101
Stam
shrb
Vps60
Mvb12
Vps28
Vps2
Vps20
Hrs
lsn
min
Relative expression
max
max
min
B
Spliceosomal complex
hoip
l(1)G0007
Prp18
nito
Sf3b6
Wdr62
Pabp2
Sf3b5
rin
CG10418
SmD3
CG9667
tsu
c12.1
CG5808
CG4849
l(3)72Ab
Cypl
Bx42
U2af38
SmD1
Hel25E
Sf3b2
SmE
Bin1
CG11808
Prp8
SmF
LSm7
BCAS2
Sf3a2
Cbp80
SmB
mago
Syp
snf
SmD2
Prp19
CG7102
CG9344
CG6227
ncm
CG7483
Neos
Prp31
CG5641
snRNP-U1-C
lost
Pep
Zn72D
SF1
snRNP-U1-70K
U2A
nonA-l
Cbp20
CG42724
Mfap1
barc
qkr58E-1
CG7564
CG2931
CG7971
CG3198
Rbp1-like
Caper
CG2685
x16
Sf3b3
pAbp
yps
C
Oxidative phosphorylation complexes and groups
CG7834
sun
ATPsynC
blw
COX4
levy
ATPsynβ
COX6B
ATPsynB
ATPsynF
ATPsynγ
ATPsynδ
RFeSP
COX5B
ATPsynD
Cyt-c1
ND-B16.6
ND-39
COX8
ND-23
SdhA
ND-MNLL
ND-13B
ND-18
ND-B14.5A
ND-B14.5B
Cyt-c-p
COX5A
ND-75
UQCR-C1
UQCR-C2
ND-20
ND-B14.7
ND-B22
ND-51
SdhD
ND-30
ND-19
UQCR-6.4

Figure S3 – **Gene expression profiles of dynamic genes from selected terms, related to Figure 2.**

(A-C) Heat map depicting the relative expression patterns of dynamic genes belonging to the described GO terms. The magenta scale depicts the intensity of the peak expression of each gene relative to that of other genes in the group. The genes are ordered according to their developmental cluster and then by their max expression peak.

Figure S4

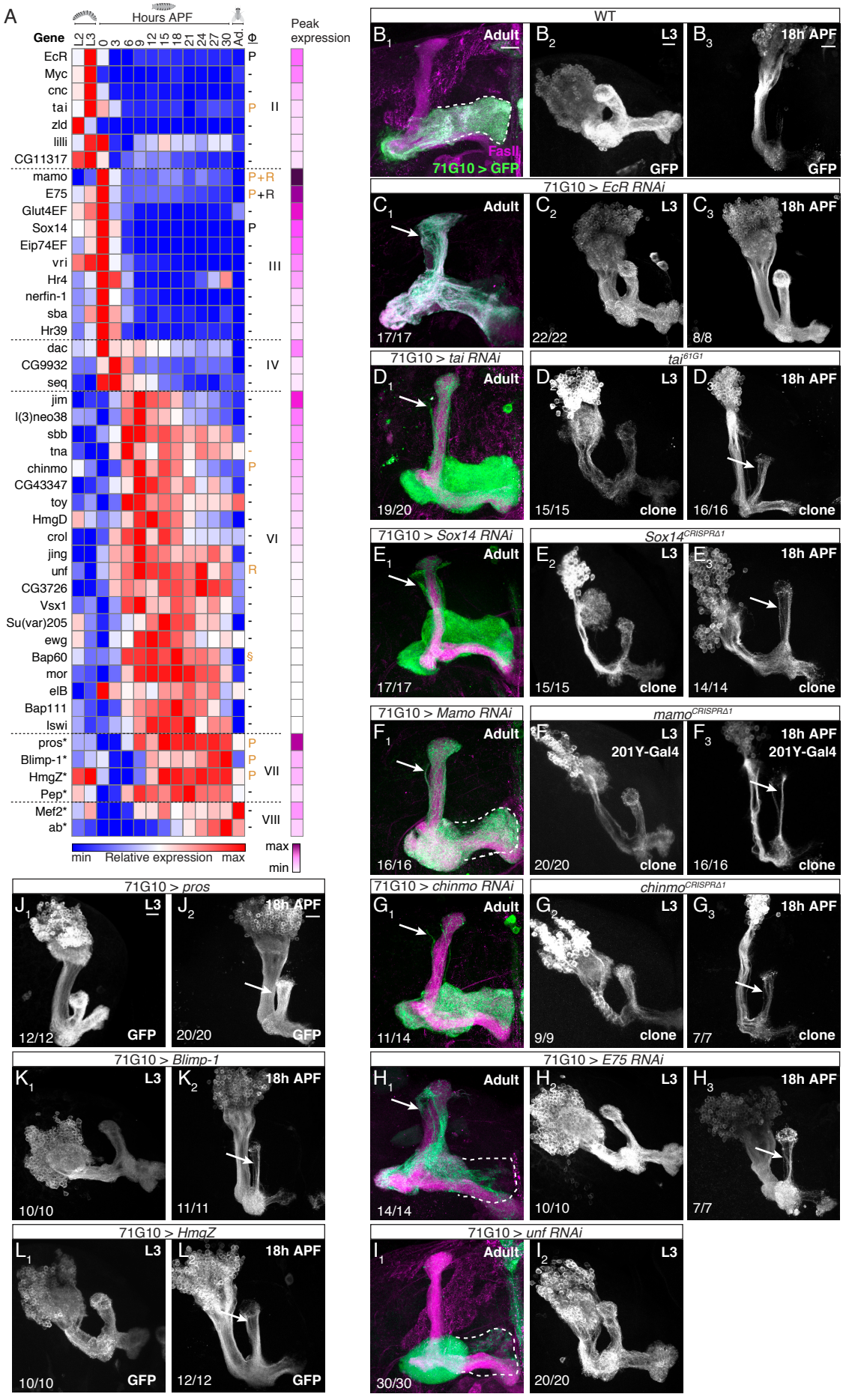
A
Hours APF
Gene
L2 L3 0 3 6 9 12 15 18 21 24 27 30 Ad.
Φ
Peak expression
EcR P
Myc -
cnc -
tai P II
zld -
lilli -
CG11317 -
mamo P+R
E75 P+R
Glut4EF -
Sox14 P
Eip74EF -
vri - III
Hr4 -
nerfin-1 -
sba -
Hr39 -
dac -
CG9932 - IV
seq -
jim -
l(3)neo38 -
sbb -
tna -
chinmo P
CG43347 -
toy -
HmgD -
crol - VI
jing -
unf R
CG3726 -
Vsx1 -
Su(var)205 -
ewg -
Bap60 §
mor -
elB -
Bap111 -
Iswi -
pros* P
Blimp-1* P
HmgZ* P VII
Pep* -
Mef2* - VIII
ab* -
min Relative expression max
max
min
WT
B1 Adult
FasII
71G10 > GFP
B2 L3
GFP
B3 18h APF
GFP
71G10 > EcR RNAi
C1 Adult
17/17
C2 L3
22/22
C3 18h APF
8/8
71G10 > tai RNAi
D1 Adult
19/20
tai61G1
D2 L3
15/15 clone
D3 18h APF
16/16 clone
71G10 > Sox14 RNAi
E1 Adult
17/17
Sox14CRISPRΔ1
E2 L3
15/15 clone
E3 18h APF
14/14 clone
71G10 > Mamo RNAi
F1 Adult
16/16
mamoCRISPRΔ1
F2 L3
201Y-Gal4
20/20 clone
F3 18h APF
201Y-Gal4
16/16 clone
71G10 > chinmo RNAi
G1 Adult
11/14
chinmoCRISPRΔ1
G2 L3
9/9 clone
G3 18h APF
7/7 clone
71G10 > pros
J1 L3
12/12 GFP
J2 18h APF
20/20 GFP
71G10 > Blimp-1
K1 L3
10/10
K2 18h APF
11/11
71G10 > E75 RNAi
H1 Adult
14/14
H2 L3
10/10
H3 18h APF
7/7
71G10 > HmgZ
L1 L3
10/10 GFP
L2 18h APF
12/12 GFP
71G10 > unf RNAi
I1 Adult
30/30
I2 L3
20/20

Figure S4 – **DNA-binding-protein screen uncovers new genes required for remodeling, related to Figure 3**

(A) Heat map of the relative expression patterns of the DNA binding proteins (DBPs) taken for the screen, sorted by cluster and peak expression levels (magenta). P, R and (-) stand for pruning, regrowth or WT phenotypes, respectively. While known roles of genes are labeled in black, new findings from this study are labeled in orange. Asterisks demarcate examples of genes whose expression is downregulated at the onset of pruning - which we therefore tested by overexpression. § demarcate the fact that while expression of Bap60 RNAi resulted in a pruning defect, we were not able to confirm this using mutant analysis.

(B-L) Confocal Z-projections of MBs of the indicated age in which 71G10-Gal4 drives the expression of mCD8-GFP as well as the indicated RNAi/overexpression transgenes (indicated by 71G10>transgene) OR, brains in which 71G10-Gal4 **(D_{2-3}**, **E_{2-3}**, **G_{2-3})** or 201Y-Gal4 **(F_{2-3})** drive the expression of mCD8-GFP within a MARCM clone of the indicated genotype.

Pruning defects are marked by arrows, and regrowth defects are evident when the adult γ lobe does not fully occupy the white dashed line. Scale bars represent 15 μm. The numbers (x/n) on the lower left corners depict the number of times the phenotype was observed out of the total hemispheres examined.

Figure S5

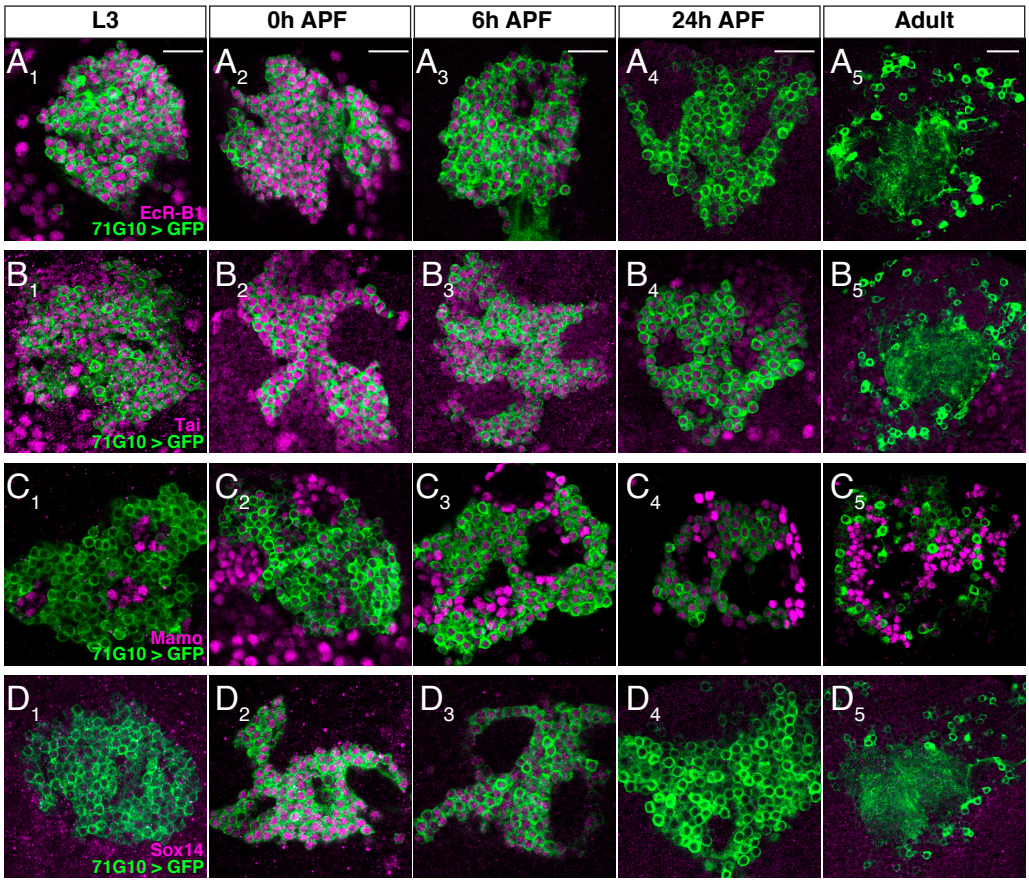
L3
0h APF
6h APF
24h APF
Adult
A1
A2
A3
A4
A5
EcR-B1
71G10 > GFP
B1
B2
B3
B4
B5
Tai
71G10 > GFP
C1
C2
C3
C4
C5
Mamo
71G10 > GFP
D1
D2
D3
D4
D5
Sox14
71G10 > GFP

Figure S5 – **Antibody staining of selected DBPs during development correlate to their RNA expression profile, related to Figure 3**

(A-D) Single confocal slices of the cell body region of MB neurons labeled with mCD8-GFP (GFP, green) driven by 71G10-Gal4 co-stained using the indicated antibodies (magenta) at the indicated developmental stages. Protein peak expression within γ neurons that are labeled in green, for each of the DBPs (0h APF for EcR-B1 and Tai, 6h APF for Mamo and 0h APF for Sox14) correlates to the RNA expression peak as referred from the RNA-seq. n>8 lobes for each experiment, scale bars represent 15 μm.

Figure S6

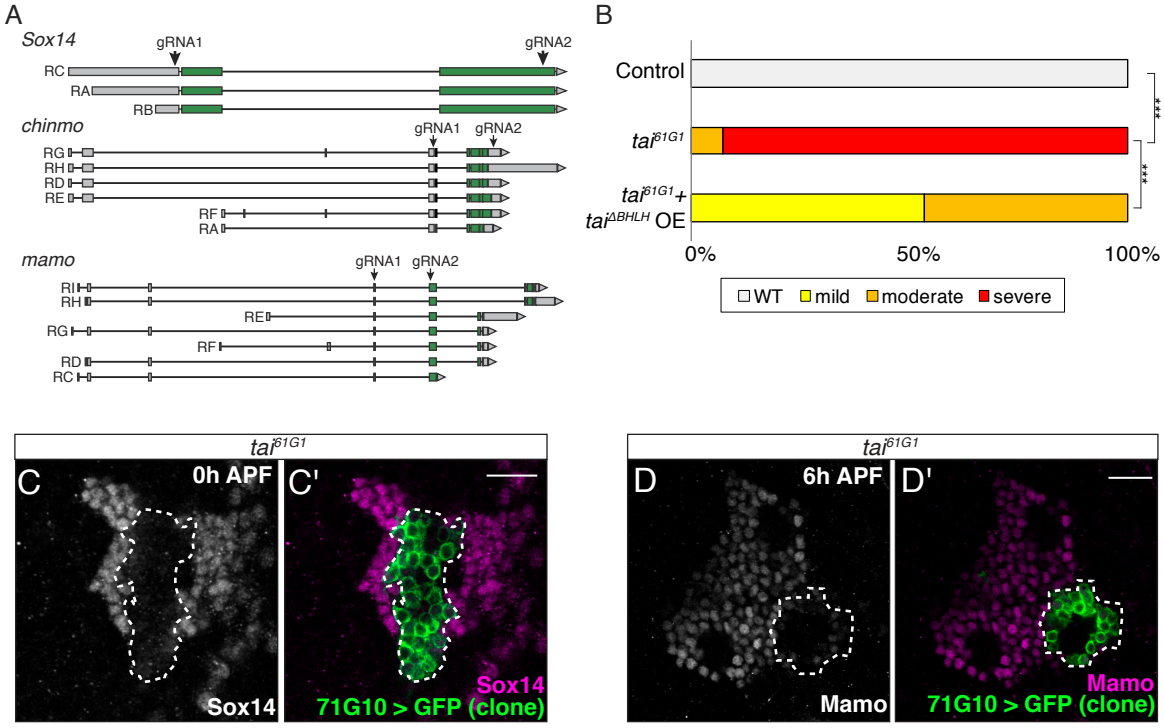
A
Sox14
gRNA1
gRNA2
RC
RA
RB
chinmo
gRNA1
gRNA2
RG
RH
RD
RE
RF
RA
mamo
gRNA1
gRNA2
RI
RH
RE
RG
RF
RD
RC
B
Control
tai61G1
tai61G1+
taiΔBHLH OE
0%
50%
100%
WT
mild
moderate
severe
***
***

tai61G1
C
0h APF
Sox14
C'
Sox14
71G10 > GFP (clone)

tai61G1
D
6h APF
Mamo
D'
Mamo
71G10 > GFP (clone)

Figure S6 – **CRISPR mediated deletion design, and *tai* function at the same epistatic level as EcR, related to Figure 3**

(A) A schematic representation of the gRNA design to induce CRISPR/Cas9-mediated deletions in *Sox14*, *chinmo* and *mamo*. Green bars represent coding exons, grey bars represent non-coding exonal sequences and lines represent introns. All annotated isoforms for each gene are displayed – while $Sox14^{CRISPR\Delta 1}$ and $chinmo^{CRISPR\Delta 1}$ alleles are deletions of most of the coding sequence, $mamo^{CRISPR\Delta 1}$ allele induces a frameshift 11 base pairs downstream of the annotated ATG (resulting in a premature stop codon). The gRNAs were designed to delete most of the coding sequence of the gene.

(B) Quantification of the pruning severity in Figure 3D, 3H and 3O using blind ranking analysis of the described genotypes. *** $p<0.001$, See experimental procedures for details.

(C-D) Single confocal sections of the cell body region of tai^{61G1} MARCM MB neuroblast clones stained for anti-Sox14 **(C,** n=6**)** or anti-Mamo **(D**, n=4**)** at 0h APF and 6h APF, respectively. Expression of Sox14 **(C)** and Mamo **(D)** is 4.2-fold ($p<0.001$) and 2.4-fold ($p<0.01$) decreased within the tai^{61G1} clone, respectively. Dashed lines demarcate the boundaries of the clone. Green represents mCD8-GFP driven by 71G10-Gal4, magenta represents Sox14 **(C)** or Mamo **(D)** antibody staining, which are also shown in grey. Scale bars represent 15 µm.

Figure S7

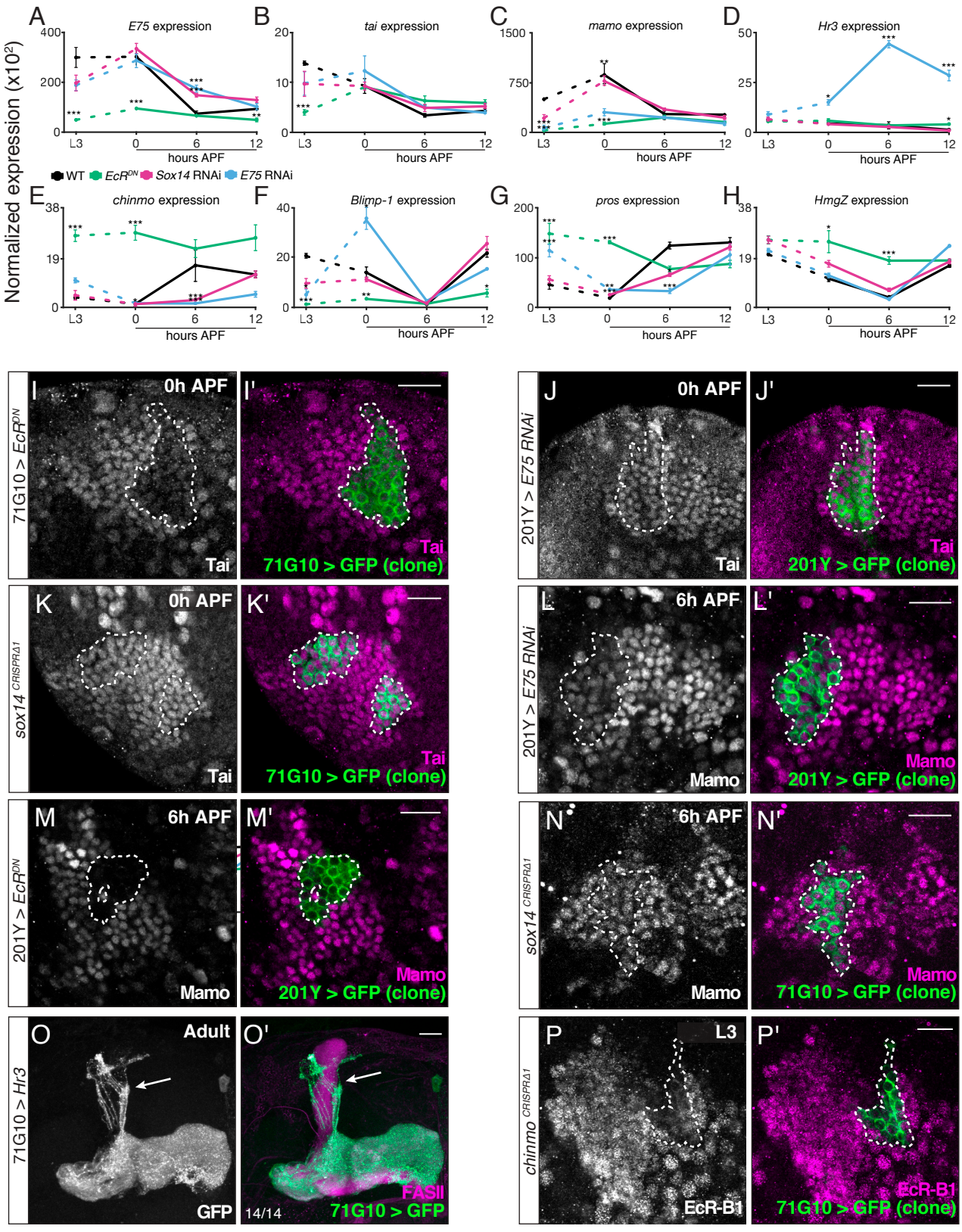
A
E75 expression
B
tai expression
C
mamo expression
D
Hr3 expression
Normalized expression (x10²)
hours APF
WT
EcR^DN
Sox14 RNAi
E75 RNAi
E
chinmo expression
F
Blimp-1 expression
G
pros expression
H
HmgZ expression
I
0h APF
Tai
I'
Tai
71G10 > GFP (clone)
71G10 > EcR^DN
J
0h APF
Tai
J'
Tai
201Y > GFP (clone)
201Y > E75 RNAi
K
0h APF
Tai
K'
Tai
71G10 > GFP (clone)
sox14 CRISPRΔ1
L
6h APF
Mamo
L'
Mamo
201Y > GFP (clone)
201Y > E75 RNAi
M
6h APF
Mamo
M'
Mamo
201Y > GFP (clone)
201Y > EcR^DN
N
6h APF
Mamo
N'
Mamo
71G10 > GFP (clone)
sox14 CRISPRΔ1
O
Adult
GFP
O'
FASII
14/14
71G10 > GFP
71G10 > Hr3
P
L3
EcR-B1
P'
EcR-B1
71G10 > GFP (clone)
chinmo CRISPRΔ1

Figure S7 – **Expression profiles of neurons perturbed for key transcription factors uncovers hierarchical regulation of axon pruning by regulatory factors, related to Figure 5**

(A-H) Normalized expression of *E75* **(A),** *tai* **(B)**, *mamo* **(C)**, *Hr3* **(D)**, *chinmo* **(E)**, *Blimp-1* **(F)**, *prospero* **(G)** or *HmgZ* **(H)** in WT MB γ neurons and in those expressing the indicated transgene (* p<0.05, ** p<0.01, *** p<0.001). Error bars indicate SEM, units on the y axis are arbitrary.

(I-N, P) Single confocal slices of MB cell bodies containing MARCM clones labeled with mCD8-GFP (GFP) driven by 71G10 **(I,K,N,P)** or 201Y **(J,L-M)** additionally expressing EcR^{DN} (**I**, n=6, **M**, n=4), *E75*-RNAi (**J**, n=8, **L**, n=8), homozygous for $Sox14^{CRISPR\Delta1}$ (**K**, n=9, **N**, n=6) or homozygous for $chinmo^{CRISPR\Delta1}$ (**P**, n=3) stained using the indicated antibody at the indicated developmental stage. The anti-Tai staining was decreased by 3.1-fold (p<0.001) within clones expressing EcR^{DN} **(I)**. The anti-Mamo staining was decreased by 2.2-fold (p<0.01) within clones expressing *E75*-RNAi **(L)** and by 7.1-fold within clones expressing EcR^{DN} **(M)**. The anti-EcR-B1 staining was decreased by 3.5-fold (p<0.001) within clones expressing $chinmo^{CRISPR\Delta1}$. The boundaries of the clones are represented by dashed lines.

(O) Confocal Z-projections of an adult MB labeled by 71G10-Gal4 driving the expression of mCD8-GFP and an *Hr3* transgene. Arrow indicates dorsally projecting unpruned γ axons. The numbers (x/n) on the lower left corners depict the number of times the phenotype was observed out of the total hemispheres examined.

Green represents mCD8-GFP expression driven by the indicated Gal4. Magenta and Gray represent the antibody indicated. Scale bars represent 15 μm.

Table S2 – Enrichment analysis of selected GO, KEGG and Reactome terms within developmental clusters

Cluster	Genes within cluster	Selected enriched terms	Term enrichment (see below)	Adjusted p value=
I	266	Synaptic transmission [GO:0007268]	35/184	5×10^{-13}
		Regulation of neurotransmitter levels [GO:0001505]	21/86	4×10^{-9}
		Voltage-gated cation channel activity [GO:0022843]	10/26	4×10^{-6}
II	188	Glycolytic process [GO:0006096]	10/16	7×10^{-7}
III	270	Proteasome-mediated ubiquitin-dependent protein catabolic process [GO:0043161]	38/123	4×10^{-22}
		Neuron projection morphogenesis [GO:0048812]	35/401	4×10^{-4}
IV	404	Programmed cell death [GO:0012501]	32/196	7×10^{-4}
		Autophagy [GO:0006914]	29/116	2×10^{-7}
		Endosome transport via multivesicular body sorting pathway [GO:0032509]	8/16	8×10^{-4}
		Endosomal transport [GO:0016197]	15/65	0.014
V	239	COP9 signalosome [GO:0008180]	6/9	1×10^{-5}
VI	309	Axon guidance [GO:0007411]	24/182	4×10^{-4}
		Axon development [GO:0061564]	28/242	3×10^{-4}
		Spliceosomal complex [GO:0005681] Spliceosome (map03040)	32/140 25/97	3×10^{-13} 2×10^{-10}
		Chromatin remodeling [GO:0006338]	19/78	2×10^{-7}
VII	247	Protein processing in endoplasmic reticulum [map04141]	13/96	0.002
VIII	316	Cellular respiration [GO:0045333]	21/79	1×10^{-7}
		Mitochondrial part [GO:0044429]	46/196	3×10^{-13}
IX	333	Synaptic transmission [GO:0007268]	34/184	7×10^{-10}
		Neurotransmitter secretion [GO:0007269]	18/80	1×10^{-5}
X	101	Ribosome [GO:0005840]	25/55	1×10^{-13}

Enrichment analysis of selected GO, KEGG and Reactome terms that are significantly enriched ($p<0.05$) after Holm–Bonferroni correction. Term enrichment refers to the number of term related genes within the cluster out of all of the *Drosophila* term related genes has significant expression in the γ neurons.

Table S6 – Enrichment analysis of selected GO, KEGG and Reactome terms within sub-clusters

Cluster	Genes within cluster	Selected enriched terms	Term enrichment	Adjusted p value=
Ia	72	Synaptic transmission [GO:0007268]	12/35	9×10^{-4}
Ib	75	Plasma membrane proton-transporting V-type ATPase complex [GO:0033181]	6/9	1×10^{-6}
Ic	43	Voltage-gated cation channel activity [GO:0022843]	5/10	1×10^{-4}
IIa	45	Glycolytic process [GO:0006096]	8/10	2×10^{-10}
IIb	38			
IIc	61			
IIIa	65	Proteasome complex [GO:0000502]	29/32	4×10^{-49}
IIIb	32			
IIIc	47	Neuron projection morphogenesis [GO:0048812]	13/35	0.003
IVa	125	Autophagy [GO:0006914]	14/29	1×10^{-4}
		ESCRT complex [GO:0036452]	4/7	0.035
		Endosome [GO:0005768]	10/26	0.01
IVb	101	programmed cell death involved in cell development [GO:0010623]	9/21	0.01
		Peptidase family C14A, cysteine active site [IPR033139]	3/3	0.01
IVc	33	Ferritin complex [GO:0070288]	2/2	0.009
Va	39			
Vb	63	RHO GTPases Activate Formins [R-DME-5663220]	3/3	0.048
VIa	36	Chromatin organization [GO:0006325]	10/41	0.01
VIb	35	Protein processing in endoplasmic reticulum [map04141]	7/13	3×10^{-4}
VIIa	47			
VIIc	40			
VIIIa	122	Mitochondrial part [GO:0044429]	23/46	6×10^{-7}
		Citrate cycle TCA cycle [map00020]	6/11	0.02
VIIIb	38			
IXa	135	Synaptic transmission [GO:0007268]	19/34	2×10^{-6}
IXb	57	Cation channel complex [GO:0034703]	4/8	0.049

Enrichment analysis of selected GO, KEGG and Reactome terms that are significantly enriched ($p<0.05$) after Holm–Bonferroni correction. Term enrichment refers to the number of term related genes within the cluster out of the number of genes from the functional group within the parent cluster.